

- ⁹A. Hoyt, Phys. Rev. 40, 477 (1932).
¹⁰R. W. Jewell, W. John, R. Massey, and B. G. Saunders, Nucl. Instr. Methods 62, 68 (1968). The "pedestal" on the γ -ray line shape mentioned in Ref. 10 has since been traced to a slit edge-penetration effect and has been eliminated by a simple modification of the slit.
¹¹G. C. Nelson, B. G. Saunders, and W. John, University of California Radiation Laboratory, Report No. UCRL-71746 (report prior to publication).
¹²W. F. Edwards, Ph.D. thesis, California Institute of Technology, Pasadena, Calif., 1960 (unpublished).
¹³J. A. Bearden, Rev. Mod. Phys. 39, 78 (1967).
¹⁴A. H. Wapstra, G. J. Nijgh, and R. van Lieshout, Nuclear Spectroscopy Tables (North-Holland Publishing Co., Amsterdam, 1959).
¹⁵R. E. Price, H. Mark, and C. D. Swift, Phys. Rev. 176, 3 (1968).

Hyperfine Structure of the Ground State of ${}^3\text{He}^+$ by the Ion-Storage Exchange-Collision Technique*

H. A. Schuessler,† E. N. Fortson, and H. G. Dehmelt

Department of Physics, University of Washington, Seattle, Washington 98105

(Received 13 March, 1969)

The hfs of the ground state of ${}^3\text{He}^+$ has been studied using the spin-dependent collision processes between stored ${}^3\text{He}^+$ ions and a polarized beam of Cs atoms. All possible hfs transitions have been measured in a magnetic field of about 7.13 G. A consecutive-pulse multiple-resonance scheme was developed to detect the only weakly field-dependent transition ($F=0$, $m_F=0$) \leftrightarrow ($F=1$, $m_F=0$) in an almost ideally isolated and pure atomic system. Magnetic-resonance disorientation is observed as a change in the number of ions remaining in the rf quadrupole ion trap after a fixed interaction time with both the resonant rf fields and the polarized atomic beam. For the detection of an ion-number signal, the ion macromotion at $\bar{\omega}_z$ was coherently excited by a homogeneous electric field at $\bar{\omega}_z + \Omega$, where Ω is the frequency of the inhomogeneous rf field used for trapping. Linewidths of 10 Hz have been measured for the (0,0) \leftrightarrow (1,0) hfs transition, when the transition was induced during a time of the order of half the electron-spin orientation time in a weak atomic beam. The value for the zero-magnetic-field hfs splitting is $\Delta\nu = (8\,665\,649\,867 \pm 10)$ Hz. Rate equations for the populations of the hfs Zeeman levels in the presence of the polarized atomic beam and transitions caused by various rf fields are given. Features of the line shape caused by the consecutive-pulse multiple-resonance scheme are also considered. Several mechanisms which may ultimately limit the precision are discussed. A comparison of the experimental result with current theories of the hfs of hydrogenic systems is presented.

OUTLINE

- | | |
|-----------------------------------------------------------------------------------------------------------------------------------------------------------------------------------------------------------------------------------------------------------------------------------------------------------------------------------------------------------------------------------------------------------------------------|-------------------------------------------------------------------------------------------------------------------------------------------------------------------------------------------------------------------------------------------------------------------------------------------------------------------------------------------------------------------------------------------------------------------------------------------------------------------------------|
| <p>I. Introduction</p> <p>II. Theory of the Experiment</p> <p>A. hfs of the $1s^2S_{1/2}$ Ground State</p> <p>B. Spin-Dependent Collision Processes</p> <p>C. Consecutive-Pulse Multiple-Resonance Scheme</p> <p>D. Rate Equations</p> <p>E. Line-Shape Considerations and Transition Probabilities</p> <p>F. Electrodynamic Ion Storage</p> <p>III. Apparatus</p> <p>A. Vacuum System</p> <p>B. Ion Storage</p> | <p>C. Cesium Beam</p> <p>D. Magnetic Field</p> <p>E. Ion Trap Electronics</p> <p>F. Microwave Generation and Stabilization</p> <p>G. Spectral Purity</p> <p>H. Frequency Measurement</p> <p>I. Microwave Field Geometry</p> <p>IV. Manipulation of Stored Charge</p> <p>A. Excitation of Coherent Ion Motion</p> <p>B. Detection of the Ion-Number Signal</p> <p>C. Effect of the Ion Space Charge</p> <p>V. Measurements</p> <p>A. Detection Procedure</p> <p>B. Results</p> |
|-----------------------------------------------------------------------------------------------------------------------------------------------------------------------------------------------------------------------------------------------------------------------------------------------------------------------------------------------------------------------------------------------------------------------------|-------------------------------------------------------------------------------------------------------------------------------------------------------------------------------------------------------------------------------------------------------------------------------------------------------------------------------------------------------------------------------------------------------------------------------------------------------------------------------|

- VI. Discussion of Possible Frequency Shifts
 - A. Stark Effect of the Containing Electric Fields
 - B. Dependence on External Magnetic Fields
 - C. Motional Magnetic Field
 - D. First-Order Doppler Shift
 - E. Second-Order Doppler Shift
 - F. Spin-Exchange Shifts
- VII. Contributions to Linewidth
 - A. Ion Storage Time
 - B. Magnetic Field Broadening
 - C. Doppler Broadening
 - D. Interaction with Atomic Beam
- VIII. Comparison with Theoretical Calculations of hfs Splitting
 - A. Ground-State Splitting Including Nuclear Structure
 - B. Ratio of ${}^3\text{He}^+$ hfs Splittings in 1S and 2S States
- IX. Future Developments
- X. Explanation of Symbols
 - A. Latin Letters
 - B. Greek Letters

I. INTRODUCTION

It has been recognized for many years that advances in high-precision rf spectroscopy have many applications both in the development of atomic clocks and in the study of atomic and of nuclear structures. The attainable precision depends ultimately upon the relative linewidth and purity of the transitions observed.

A method developed in our laboratory in recent years for the spectroscopy of paramagnetic atomic ions is ideally suited in both these respects and is difficult to match by other magnetic resonance techniques. We named this technique the ion storage exchange collision (ISEC) method. The atomic ions are confined by electric fields in high vacuum and are practically free from environmental perturbations which might otherwise broaden and shift the magnetic resonance lines.

This paper describes a measurement of the hfs splitting in ground-state ${}^3\text{He}^+$ ions. The present measurement provides the first demonstration of the high resolution and high intrinsic accuracy inherent in the ISEC technique.

${}^3\text{He}^+$ was selected as the first ion for study since its simple, hydrogenlike, structure makes it, theoretically, the most interesting atomic ion. Accurate theoretical evaluations of the hfs in ${}^3\text{He}^+$ enable us to use our experimental hfs values to study the ${}^3\text{He}^+$ nuclear structure and to test certain quantum electrodynamic corrections to the hfs of hydrogenic systems. The ratio of our ground-state hfs value to the hfs splitting measured in the 2S metastable state of ${}^3\text{He}^+$ by Novick and Commins¹ is of particular interest. In this

ratio, the nuclear structure effects cancel out to a high order, permitting a direct and accurate test of purely electrodynamic corrections.

The present experiment is a culmination of a sequence of earlier studies, which began with the utilization of exchange collisions in the spin resonance of electrons held in a dilute plasma.² Next, attention was focused on the field confinement of atomic ions in high vacuum and the study of their rf spectrum through spin-dependent collisions with a spin polarized atomic beam. The latter technique first proved successful in the case of ${}^4\text{He}^+$ ions,³ which paved the way for our study of the ${}^3\text{He}^+$ hfs. A detailed description of the method and of some of the apparatus we used has already appeared in connection with the ${}^4\text{He}^+$ work.⁴ In addition, a general analysis of the properties of stored ions and methods of obtaining their rf spectra is being published.⁵ A report on our preliminary measurements of the hfs of ${}^3\text{He}^+$ has also been presented.⁶

For the present experiment, a number of important changes has been made on the apparatus and in the technique. In order to observe the magnetic-resonance transition with minimal shifts a new consecutive-pulse multiple-resonance scheme had to be developed. A new detection scheme proved more favorable for achieving a signal-to-noise ratio limited essentially by the statistical ion noise. A digital analyzer was used for signal averaging. Reconstruction of the beam source and of the electron-gun pulser stabilized the general performance.

A brief review of the principles of the ISEC method follows. References 4 and 5 may be consulted for further details.

${}^3\text{He}^+$ ions are created in a Paul-Fischer rf quadrupole ion trap by pulsed electron bombardment of the background ${}^3\text{He}$ atoms. An optically pumped beam of Cs atoms, passing through the trap, imparts a spin orientation to the ions by spin exchange. At the same time, the spin-dependent charge exchange reaction between Cs and ${}^3\text{He}^+$ reduced the ${}^3\text{He}^+$ ion population in the trap at a rate determined by the spin states of the ${}^3\text{He}^+$. Thus, by detecting the number of ions remaining in the trap after a fixed period of interaction with the Cs beam, one has a measure of the spin polarization of the He ions and can detect a resonant depolarization caused by rf transitions.

II. THEORY OF THE EXPERIMENT

A. Hfs of the $1s^2S_{1/2}$ Ground State

For a system with nuclear spin I and electronic angular momentum J , the Hamiltonian is particularly simple when I or $J < \frac{1}{2}$ since the quadrupole interaction vanishes in such cases.

$$\mathcal{H} = A\vec{I}\vec{J} + \mu_0 g_J \vec{J}\vec{H}_0 + \mu_0 g'_I \vec{I}\vec{H}_0 \quad (2.1)$$

In this expression, the first term is the magnetic dipole interaction of the nucleus with the magnetic field of the electron shell. The magnetic dipole splitting factor A is directly proportional to the nuclear moment μ_n and to the expectation value of the magnetic field of the electrons at the nucleus $\langle H(0) \rangle$ and is inversely proportional to I and J . The second and third terms represent the interaction of the electrons and the nucleus with the external magnetic field. The energy eigenvalues are given by the well-known Breit-Rabi formula. A hyperfine energy-level diagram is plotted in Fig. 1. The abscissa shows the dimensionless parameter $x = (g_J - g_I')\mu_0 H_0 / \Delta W$. Due to the negative magnetic moment of the ${}^3\text{He}$ nucleus, the level with the largest F has the lowest energy, which corresponds to an inverted term sequence.

All possible transitions are indicated and were actually observed. Expressed in low-field quantum numbers $(F, m_F) \leftrightarrow (F', m_{F'})$, the enumeration is as follows:

$$\begin{aligned} (0, 0) &\leftrightarrow (1, 1) \text{ at } \nu_a = \Delta\nu - \nu_z + \delta, \\ (0, 0) &\leftrightarrow (1, 0) \text{ at } \nu_b = \Delta\nu + 2\delta, \\ (0, 0) &\leftrightarrow (1, -1) \text{ at } \nu_c = \Delta\nu + \nu_z + \delta, \\ (1, 1) &\leftrightarrow (1, 0) \text{ at } \nu_d = \nu_z + \delta, \\ (1, 1) &\leftrightarrow (1, -1) \text{ at } \nu_e = \nu_z, \\ (1, 0) &\leftrightarrow (1, -1) \text{ at } \nu_f = \nu_z - \delta. \end{aligned} \quad (2.2)$$

$\Delta\nu$ is the zero-field hfs separation which, for ${}^3\text{He}^+$ with $I = J = \frac{1}{2}$, is given by $\Delta\nu = A/h$. The double quantum transition frequency ν_z can be written $\nu_z = |(g_J + g_I')\mu_0 H_0 / 2\hbar$. With weak magnetic field strengths, the small field-dependent contribution δ may be expressed by use of the Breit-Rabi formula up through terms of the order of H^2 and is

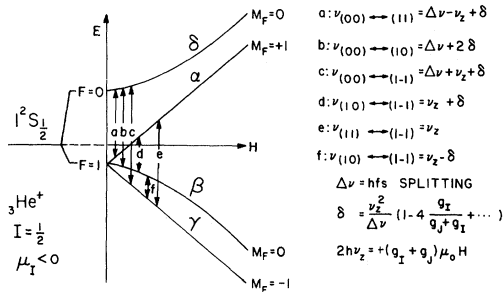


FIG. 1. Breit-Rabi diagram of the ${}^2S_{1/2}$ ground state of ${}^3\text{He}^+$. All possible transitions were observed and are shown. The double quantum transition, denoted by e , was strongest when typical rf field strengths were used.

$$\delta = \nu_z^2 (1 - 4g_I'g_J) / \Delta\nu. \quad (2.3)$$

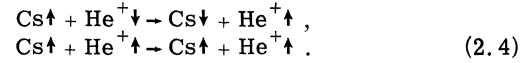
The narrow double quantum transition was used to determine the magnetic field in frequency units.

The observation of the field-dependent magnetic dipole transitions was made in a conventional way by applying rf fields of proper frequency and direction. With the static magnetic field inclined by 45° with respect to the rf magnetic field, it is possible to excite both σ and π transitions in the same apparatus. For the ${}^3\text{He}^+$ ground state all field-dependent lines are π transitions, having the low-field selection rules $\Delta F = 0, \pm 1$ and $\Delta m_F = \pm 1$. To obtain a highly precise value for the zero-field hfs splitting, $\Delta\nu$, the almost field-independent b transition $\Delta F = \pm 1$, $\Delta m_F = 0$, was of primary interest. A more complex transition scheme had to be developed to detect this σ transition. This consecutive-pulse multiple-resonance scheme is described in Sec. II C.

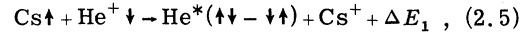
B. Spin-Dependent Collision Processes

Since the various spin-dependent collision processes have already been described in detail,⁴ the procedure is only outlined and the results are summarized in the following.

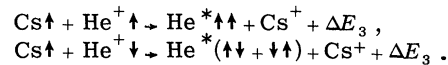
The purpose of the polarized alkali atomic beam is twofold: firstly, to transfer polarization to the stored ions by spin exchange. In this process, $I=0$ He^+ ions become oriented, whereas polarization of the Cs atoms is lost:



In a simultaneous second process, the ion polarization is detected by charge exchange. The neutralization rate depends on the relative orientation of the electronic spins of the collision partners and occurs along a fast singlet channel



and slow triplet channels



The ΔE_i are the ionization energy differences for the singlet and triplet charge-exchange reactions.

Whereas, for the spin-exchange collisions, most alkali atoms would be practical, the specific choice of Cs as a collision partner for He^+ was made because of the expected favorably large dependence of the charge exchange and, therefore, of the ion lifetime on the relative electron-spin orientation. According to Rapp and Francis,⁷ the charge-exchange cross section depends on the

small energy defect ΔE , the relative velocity of the collision partners, and on the ionization energy I of the ground-state Cs atom and of the excited He^* atom.

Figure 2 shows excited fine-structure levels of the He atom nearest to the ground state of Cs. The Cs ground state is almost resonant with both the 1S_0 and the 3P_1 first excited states of He. The difference in the ionization energies of $\Delta E_1 = 0.08$ eV and $\Delta E_3 = -0.26$ eV, and a typical relative velocity of $\sim 10^6$ cm/sec, leads to a singlet charge exchange cross section Q_1 which is about 20 times larger than the triplet cross section Q_3 . Also, the charge exchange cross section $Q(\Delta E = 0)$ may be taken as a lower limit for the spin-exchange cross section $Q_e \geq 30 Q_1$.

The order of magnitude differences in the cross sections $Q_e \gg Q_1 \gg Q_3$ ensure that the ions assume about the same polarization as the incident atoms during a time which is short against their neutralization time. In this case, ions with spins parallel to the spins of the atomic beam atoms have longer lifetimes than ions with antiparallel spins.

The time evolution of the ion number n of polarized He^+ under the influence of charge-exchange collisions with the polarized Cs beam is described by charge-exchange rate equations in terms of the spin polarizations $\langle s_z \rangle / s$, which are labeled p for ions and P for atoms. The change of the stored ion number n is given by

$$dn/dt = -(n/T_0)[1 - pP(\Delta Q/4\bar{Q})]. \quad (2.6)$$

Here T_0 is the average ion lifetime for a given unpolarized atomic beam, $\Delta Q = Q_1 - Q_3$, and $\bar{Q} = \frac{1}{4}(Q_1 + 3Q_3)$.

In the experiment, a polarization signal $S(p, P)$, defined as the relative difference in ion

numbers remaining in the trap after a time t with collision partners either polarized or unpolarized, was measured,

$$S(p, P) = [n(p, P) - n(0, 0)]/n(0, 0). \quad (2.7)$$

Assuming only statistical fluctuations, the polarization signal $S[p(t), P(t)]$ has an optimum value of

$$S^*(p, P) = \frac{1}{2} pP(\Delta Q/\bar{Q}), \quad S^* \ll 1 \quad (2.8)$$

for $t = 2T_0$. The polarization signal disappears when either p or P are destroyed. P is easily destroyed by applying the Zeeman frequencies of the Cs ground state. The $^3\text{He}^+$ ions become completely disoriented, with $p = 0$, by a saturating rf field at the double quantum transition frequency, but only partly disoriented, with $p > 0$, when the other hfs resonance frequencies are applied. The occurrence of b transitions alone does not change the polarization p at all. Analogous to Eq. (2.7), therefore, we may define a rf transition signal S'_i as the relative difference in remaining ion numbers with and without a rf field on resonance.

In terms of the applied frequency, S'_i is

$$S'_i = [S(P, P) - S(p_i, P)]/S(P, P) \\ = [n(P, P) - n(p_i, P)]/[n(P, P) - n(0)] = 1 - p_i/P. \quad (2.9)$$

Here, p_i is the reduced ion polarization for a rf field which is resonant at the transition frequency labeled i . The dependence of the transition reduced ion polarization on the total ion polarization is discussed in Sec. II D.

C. Consecutive-Pulse Multiple-Resonance Scheme

$\Delta m_F = 0$ transitions alone do not influence the polarization. Therefore, their effect in connection with suitably chosen directly observable $|\Delta m_F| = 1$ transitions was used. We have developed a new consecutive-pulse multiple-resonance scheme to eliminate undesirable frequency pulling and line broadening effects, which are believed to affect the b -transition frequency in the previous simpler simultaneous scheme.⁶

The principle of the new scheme is illustrated in Fig. 3. A diagram of the participating hfs levels, the sequence of pulses, the development of the instantaneous polarization p and of the average polarization \bar{p} , as a function of time, are depicted. The scheme consists of applying consecutively three rf pulses. The first pulse, centered at the d -transition resonance frequency, is short against the spin-exchange time. The pulse width has been adjusted to cause the populations of the α and β states to be inverted at the

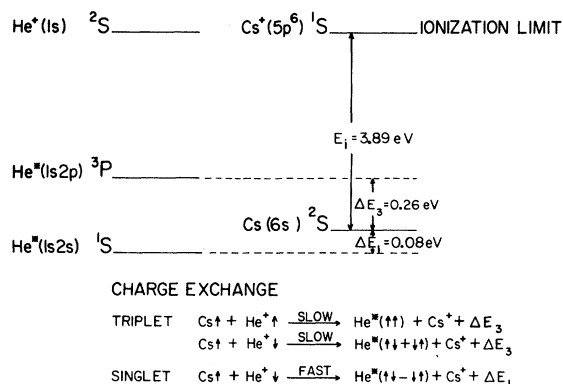


FIG. 2. Fine-structure levels of the He and Cs atoms participating in the almost resonant charge exchange (level separations are not to scale).

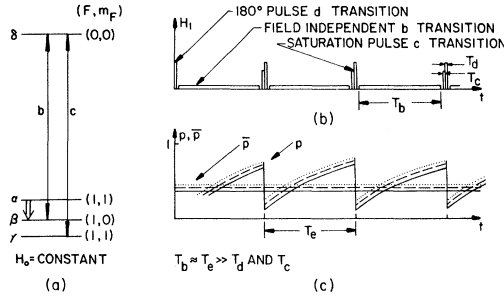


FIG. 3. Consecutive-pulse multiple-resonance scheme developed to make the b transition directly observable. (a) Diagram of involved hfs levels. (b) Sequence of the b , c , d pulses. T_b , T_c , T_d are, respectively, the duration of the b , c , and d transition pulses. H_1 is the amplitude of the applied rf field. (c) Time evolution of the instantaneous ion polarization p and the average ion polarization \bar{p} . Three cases are shown schematically. The dotted curves represent the case in which only the d pulse was applied. The dashed curves illustrate the case in which the d - and b -transition pulses were applied consecutively. The solid curves show the complete pulse scheme, when the d -, b -, and c -transition pulses were applied in sequence.

end of each pulse. We call this pulse a 180° pulse since the reversal of the occupation numbers is analogous to a 180° precession of the macroscopic polarization at angular frequency ω_1 in a two-level system. The pulse height H_1 and the width T_d fulfill the relation

$$\omega_1 T_d = \gamma H_1 T_d = \pi, \quad T_d \ll T_e. \quad (2.10)$$

The third pulse saturates the c transition. The field-independent b transition of interest is induced by the central pulse. The duration of the outer $\Delta m_F = \pm 1$ pulses is very short compared to the central pulse, which is applied over one spin-exchange period in a weak atomic beam. Typical pulse widths are 0.2 msec for the 180° pulse at the d transition, 3.2 msec for the c transition saturation pulse, and 76.6 msec for the central b transition pulse.

For the purpose of explanation, the ideal case of atomic beam and, therefore, ion polarization both being initially 1 is considered. The process is described in three steps and for each step the evolution of both instantaneous polarization p and average polarization \bar{p} are shown.

First, only the 180° pulse is applied. If no magnetic dipole transitions occur during the times of the second pulse, for instance, when the frequency is off-resonance, the spin-exchange process tends to pump the ions back into the initial α -state until the next 180° pulse interchanges the population numbers of the α and β states.

This situation is indicated by dotted lines. The net effect is a decrease in the average ion polarization \bar{p} and is shown by the horizontal line in the graph of the time evolution of p in Fig. 3.

In the next step, the frequency of the b transition is on-resonance during the second pulse. There is now a certain probability that ions are sorted out into the δ state and are not available in the following 180° pulse. Therefore, both the instantaneous and the average polarization decrease further as shown by the dashed lines. At this stage a b -transition resonance signal may already be detected.

If, in addition, the c transition is fixed at resonance and saturated during the third pulse period, and if the b transition is also at resonance, some ions that have gone from the β to the δ state may end up in the γ state, which has a negative contribution to the polarization. Thus, the effect of the added c -saturation pulse is to reinforce the b -transition signal. This situation of the complete consecutive-pulse multiple-resonance scheme is indicated by solid lines. In a measurement, the frequency, power, and duration of the rf fields for the outer two pulses were held fixed, while the frequency of the central b -transition pulse was varied through resonance.

In principle, it should be possible to improve the pulse scheme just described slightly by applying 180° pulses also at the two microwave frequencies ($\Delta F = \pm 1$ transitions). For this purpose, the microwave field strength has to be fairly constant over the transition region, which was not the case for the present cavity construction (see Fig. 14). However, transitions induced under adiabatic fast passage conditions could be employed. The requirements are then less stringent, but rather large field strengths are needed.

D. Rate Equations

In order to quantitatively estimate the size of the various rf-transition signals, the effect of resonant rf fields on the electron-spin polarization p of the ions has to be considered. With reference to Fig. 1, the polarization of the ensemble may be defined in terms of occupation numbers and spin polarizations as

$$p = (n_\alpha p_\alpha + n_\beta p_\beta + n_\gamma p_\gamma + n_\delta p_\delta) / n. \quad (2.11)$$

In the case of the ${}^3\text{He}^+$ ground state, it is easily found that

$$p = (n_\alpha - n_\gamma) / n. \quad (2.12)$$

In Ref. 4, the following rate equations have been derived for spin-exchange collisions between at-

oms of arbitrary polarization P and ${}^3\text{He}^+$ ions

$$\begin{aligned}\dot{n}_\alpha &= -2(1-P)n_\alpha + (1+P)n_\beta + (1+P)n_\delta, \\ \dot{n}_\beta &= +(1-P)n_\alpha - 3n_\beta + (1+P)n_\gamma + n_\delta, \\ \dot{n}_\gamma &= +(1-P)n_\beta - 2(1+P)n_\gamma + (1-P)n_\delta, \\ \dot{n}_\delta &= +(1-P)n_\alpha + n_\beta + (1+P)n_\gamma - 3n_\delta.\end{aligned}\quad (2.13)$$

In deriving the equations, it is assumed that the relatively slow ion-loss processes can be neglected. This is a valid approximation because of the relative order of the spin-exchange and the charge-exchange cross sections. The time is in units of $4T_e$ with T_e being the average spin-exchange time.

It is instructive to solve these equations under steady-state conditions with disorienting rf fields either present or turned off. Without rf fields and with polarizing and relaxing effects in equilibrium, we have $\dot{n}_\alpha = \dot{n}_\beta = \dot{n}_\gamma = \dot{n}_\delta = 0$ and unnormalized occupation numbers may be found to be $n_\alpha = (1+P)/(1-P)$, $n_\gamma = (1-P)/(1+P)$, $n_\delta = n_\beta = 1$. According to this, the equilibrium ion polarization p is equal to the atomic polarization P .

The occupation numbers are modified when a resonant rf field is present. When the magnetic dipole transition i is induced, the polarization p is reduced to p_i . This transition reduced polarization is defined analogous to Eqs. (2.11) and (2.12) as

$$p_i = (n_{\alpha i} - n_{\gamma i})/n, \quad (2.14)$$

with $n_{\alpha i}$ and $n_{\beta i}$ being the transition-modified occupation numbers of the α and of the γ states. Assuming rf saturation and slow passage through resonance, the occupation numbers are in equilibrium and the rate equations are reduced to a set of linear equations. If, for example, the applied rf field is resonant between the α and β states, Eq. (2.13) has to be solved with $n_\alpha = n_\beta$ and $\dot{n}_\gamma = \dot{n}_\delta = 0$. Accordingly, it is derived that $p_d = p_a = 3P/(5+2P)$, $p_f = p_c = 3P/(5-2P)$, $p_b = P$, and $p_e = 0$. The results have been summarized in Table I. The relative signal strengths S_i' defined by Eq. (2.9) can then readily be calculated with these results for arbitrary polarization P .

From the above consideration follows also that b transitions alone may not be detected. Other internal transitions have to be additionally induced to make the system sensitive to the b -transition frequency. A simple scheme is given by simultaneously saturating the d and c transitions. If, in addition, b transitions are strongly induced, all four participating states will be equally populated and $p_{bcd} = 0$. We shall call

TABLE I. Unnormalized population numbers, transition reduced polarization, and relative signal strength of saturated rf transitions between hfs levels of ${}^3\text{He}^+$.

Transition i	Population numbers		Reduced polarization		Relative signal S_i'
	n_α	n_β	n_δ	p_i	
a	1	$(5-3P)/(5+P)$	1	$3P/(5+2P)$	$2(1+P)/(5+2P)$
b	$(1+P)/(1-P)$	1	1	P	0
c	$(1+P)(5+P)/(1-P)$	$(5+3P)/(5-P)$	1	$3P/(5-2P)$	$2(1-P)/(5-2P)$
d	$(5+P)/(5-3P)$	$(5+P)/(5-3P)$	1	$3P/(5+2P)$	$2(1+P)/(5+2P)$
e	1	1	1	0	1
f	$(5+P)(1+P)/(5+3P)$	$(5-P)/(5+3P)$	1	$3P/(5-2P)$	$2(1-P)/(5-2P)$
$c+d$	$(3+2P)/(3-2P)$	$(3+2P)/(3-2P)$	1	$P/3$	$1-P/3$
$b+c+d$	1	1	1	0	1
none	$(1+P)/(1-P)$	1	1	P	1

this scheme the basic scheme to distinguish it from the pulsed scheme.

In order to discuss the size of the expected resonance effect in this basic scheme, we shall have to compare p_{bcd} with the corresponding transition reduced polarization p_{cd} for the case that the b transition is off-resonance or turned off.

We begin with an extension of the rate equations (2.13) to derive p_{cd} . The extension is made to take into account the existence of two simultaneous rf "relaxations." The rf-induced changes of the occupation numbers are

$$\begin{aligned} \dot{n}_{\alpha d} &= \lambda_d (n_\alpha - n_\beta), & \dot{n}_{\beta d} &= \lambda_d (n_\beta - n_\alpha), \\ \dot{n}_{\gamma c} &= \lambda_c (n_\gamma - n_\delta), & \dot{n}_{\delta c} &= \lambda_c (n_\delta - n_\gamma). \end{aligned} \quad (2.15)$$

The rate of induced transitions λ_d and λ_c is assumed to be high enough, so that even for nearly equal occupation numbers of rf-coupled states, the contributions $\dot{n}_{\alpha d}$, $\dot{n}_{\beta d}$, $\dot{n}_{\gamma c}$, and $\dot{n}_{\delta c}$ stay finite. Following the usual procedure, we solve for steady-state conditions $\dot{n}_i = 0$ and take simultaneously $n_\alpha = n_\beta$ and $n_\gamma = n_\delta$:

$$\begin{aligned} n_\alpha &= n_\beta = (3 + 2P)/(3 - 2P), & (2.16) \\ n_\beta &= n_\gamma = 1, \end{aligned}$$

which yields $p_{cd} = \frac{1}{3}P$ and $S'_{cd} = 1 - \frac{1}{3}$.

When all three rf transitions d , b , and c are induced, the hfs states are coupled with each other and $p_{bcd} = 0$. The relative signal strength is then $S'_{bcd} = 1$, which is the maximum signal obtainable. The signal is the same as obtained for saturation of the double quantum transition.

It is now readily seen from Eq. (2.16) that, in the basic scheme, the b -transition signal is

$$S'_{bcd} - S'_{cd} = \frac{1}{3}. \quad (2.17)$$

However, if a precision of one part per 10^9 is to be achieved, it is desirable that the observed resonance signal not be frequency shifted by the simultaneous application of several rf fields, and that line broadening effects be minimized. The choice of the consecutive-pulse multiple-resonance scheme, already described in Sec. II C, avoids these difficulties.

We shall, therefore, focus our interest now on the signal size S_i^\dagger to be expected when part of or the whole consecutive-pulse multiple-resonance scheme is applied. The following conditions are assumed:

(i) The durations of the d - and c -transition pulses are very short against the duration of the

b -transition pulse and may be regarded as instantaneous perturbations.

(ii) The field strengths of the d and c transitions have been adjusted for optimum perturbation. The b -transition field is weak and is applied during the long central-pulse period.

(iii) The spin-exchange time T_e is much smaller than the b -transition pulse time, so that the rf perturbation may be treated as a rate process.

It is in the spirit of our approximation to instantaneously perform the operations of the d - and c -transition pulses at the beginning of each consecutive pulse sequence by a proper choice of initial occupation numbers. This is possible, since the two strong rf pulses are induced at different times between different hfs levels. The effect of the long b -transition pulse will be included in the rate equations. In sufficient approximation, we seek a solution for the ideal case $P=1$, for which the incident Cs beam is completely polarized. (In the experiment, the polarization was $P=p=0.5$, which is shown later.) During the time in which the b transition takes place, the ensemble may be described by the following set of simple rate equations:

$$\begin{aligned} \dot{n}_\alpha &= 2n_\beta + 2n_\delta, \\ \dot{n}_\beta &= -3n_\beta + 2n_\gamma + n_\delta - (n_\beta - n_\delta)/T_1, & (P=1) \\ \dot{n}_\gamma &= -4n_\gamma, \\ \dot{n}_\delta &= n_\beta + 2n_\gamma - 3n_\delta + (n_\beta - n_\delta)/T_1. \end{aligned} \quad (2.18)$$

On solving one obtains

$$\begin{aligned} n_\alpha &= n_{\alpha 0} + (1 - e^{-2t})n_{\beta 0} + (1 + e^{-4t} - 2e^{-2t})n_{\gamma 0} \\ &\quad + (1 - e^{-2t})n_{\delta 0}, \\ n_\beta &= e^{-2t} \left[\frac{1}{2}(1 + e^{-2zt})n_{\beta 0} + (1 - e^{-2t})n_{\gamma 0} \right. \\ &\quad \left. + \frac{1}{2}(1 - e^{-2zt})n_{\delta 0} \right], & (2.19) \\ n_\gamma &= e^{-4t} n_{\gamma 0}, \\ n_\delta &= e^{-2t} \left[\frac{1}{2}(1 - e^{-2zt})n_{\beta 0} + (1 - e^{-2t})n_{\gamma 0} \right. \\ &\quad \left. + \frac{1}{2}(1 + e^{-2zt})n_{\delta 0} \right]. \end{aligned}$$

Here $n_{\alpha 0}$, $n_{\beta 0}$, $n_{\gamma 0}$, and $n_{\delta 0}$ are the occupation numbers at the beginning of each cycle, and $1 + (1/T_1)$ has been substituted by z with the rf-induced period of revolution T_1 being defined in units of $4T_e$ by $T_1 = 2\pi/\gamma H_1 4T_e$. Inspection of (2.19) shows that the behavior of the population numbers n_{α} , n_{β} , n_{γ} , n_{δ} becomes periodic after a few cycles of duration T_p . Correspondingly, initial and final occupation numbers quickly approach fixed asymptotic values.

Using Eqs. (2.19) and (2.14) and time averaging the evolution of the occupation numbers, yield the average reduced ion polarization \bar{p} . The quantity \bar{p} depends on the timing, frequencies, and power level of the consecutive-pulse multiple-resonance scheme, and on the Cs beam intensity. For a given weak Cs atomic beam, four separate cases are of interest: (a) 180° pulse effective, b transitions partially saturated, c transition saturated. (b) 180° pulse effective, no b transitions, c transition saturated. (c) 180° pulse effective, b transitions partially saturated, no c transitions. (d) 180° pulse effective, no b transitions, no c transition.

In order to compute the signal strength S_i^\dagger , taking the various conditions for the initial occupation numbers in each cycle into account, it is useful to make a table compiling the results of Eq. (2.19). The b field strength is chosen to fulfill the condition $T_e = 2\pi/\gamma H_1$.

In Table II, the steady-state populations and average transition reduced polarizations are listed for a pulse length of $T_p = T_e$ used for the final measurements.

The signal size S_i^\dagger is easily found for the different special cases of interest. As an example, we give the estimated size of the signal when the complete consecutive-pulse multiple-resonance scheme is employed. This quantity is obtained by subtracting the average transition reduced polarization of case b from that of case a. A comparison of the result

$$S_{bcd}^\dagger - S_{cd}^\dagger = \frac{1}{10} \quad (2.20)$$

with Eq. (2.17) shows that the high intrinsic accuracy of the pulsed scheme is obtained only at the cost of the signal size being about three times smaller in the pulsed than in the continuous scheme.

The preceding calculations are correct for $P=1$. However, according to the results obtained in Eq. (2.16) for the basic continuous scheme with arbitrary polarization, it is a reasonable approximation to assume the transition reduced polarization \bar{p}_i of the pulsed scheme to be directly proportional to the atomic beam polarization P . In this sense, the average transition reduced ion polarization \bar{p}_i has been used instead of p_i in the theoretical expression of Eq. (2.9) for the relative signal size.

From the above considerations, it seems desirable also to measure the spin-exchange time between stored ions and the polarized Cs beam. It is clear that for $^3\text{He}^+$ ions, because of the presence of a coupled nuclear spin of $I = \frac{1}{2}$ and the conservation of total angular momentum, two exchange collisions are necessary on the average to orient one $^3\text{He}^+$ ion. We have measured this orientation time $2T_e$ using the experimental conditions of case d. Hereby, the time between the short (typically 0.2 msec wide) fixed 180° pulses at the d -transition frequency was varied. For each fixed separation ranging from 2 to 160 msec the pulse train (total length 1 sec) would yield a different value for the transition reduced ion polarization. From the increase of the average transition reduced ion polarization, the electron-spin orientation time $2T_e = 90$ msec was derived for the weak Cs beam normally used. Since only the orientation time for the weak Cs beam was of interest in the present experiment, no efforts were made to determine the related absolute spin-exchange cross section.

E. Line-Shape Considerations and Transition Probabilities

For an understanding of the line shape of the expected magnetic-resonance signals, it is necessary to discuss the effects of the various applied rf

TABLE II. Steady-state populations and average transition reduced polarizations for various cases of the consecutive pulse scheme. With $T_p = T_e$, the b field strength is adjusted to yield $T_1 = T_e$. Occupation numbers are normalized according to $\sum n_i = 1$ and an atomic polarization $P=1$ is assumed.

Duration of cycle in units $4T_e$	Case	Occupation numbers in consecutive cycles								Average transition reduced polarization \bar{p}
		Beginning				End				
		$n_{\alpha 0}$	$n_{\beta 0}$	$n_{\gamma 0}$	$n_{\delta 0}$	n_{α}	n_{β}	n_{γ}	n_{δ}	
$T_p = \frac{1}{4}$	1	0.23	0.50	0.13	0.13	0.50	0.23	0.05	0.21	0.29
	2	0.30	0.56	0.07	0.07	0.56	0.30	0.03	0.12	0.39
	3	0.24	0.54	0.0	0.22	0.54	0.24	0.0	0.22	0.40
	4	0.30	0.57	0.0	0.13	0.57	0.30	0.0	0.13	0.43

fields. The line shape of the nearly field-independent b transition is of particular interest, when the consecutive-pulse multiple-resonance scheme is applied.

When the d and c transitions are very short compared with the central b transition, the period T_p for the complete scheme is practically equal to the period over which the b transition is induced (T_p is again measured in units of $4T_e$).

We shall discuss the limiting case of weak spin-exchange collisions and of a weak applied b transition field only. More specifically, our assumption is $1/T_p \gg 1/T_e$, $1/T_1$ with the spin precession rate $1/T_1$ defined as $1/T_1 = \gamma H_1/2\pi$. The following discussion of the line shape will, therefore, just be qualitative, containing, nevertheless, all features necessary for a line-shape analysis. The outer pulses are adjusted for optimum transition probability. For illustration we again consider the simple case $P=1$.

Applying the consecutive pulses, an equilibrium is soon reached, when the occupation numbers at the end and the beginning of consecutive-pulse cycles are equal. In order to evaluate the evolution of the occupation numbers, the operations of the pulse scheme have to be carried out stepwise. Hereby, the effect of the spin-exchange collisions was accounted for by linearly approximating the solutions of the spin-exchange rate equations. The following equations for the equilibrium occupation numbers n_i are obtained by equating initial and final n_i values:

$$\begin{aligned} (2T_p - 1)n_\alpha + n_\beta + 2T_p n_\delta &= 0, \\ -(3T_p - 1)n_\alpha - n_\beta + T_p n_\delta + 2T_p n_\gamma - \epsilon &= 0, \\ n_\alpha + n_\beta + 2n_\delta &= 1, \\ n_\gamma &= n_\delta. \end{aligned} \quad (2.21)$$

The term ϵ describes the effect of the weak b -transition field.

First, we solve the case that the b -transition field is off-resonance or turned off. Then with $\epsilon=0$, the occupation numbers of interest follow from Eq. (2.21) as $n_\alpha = n_\beta = 0.42$ and $n_\gamma = n_\delta = 0.08$. With the present assumption of weak spin-exchange collisions and weak rf fields, the more general integral solutions Eq. (2.19) lead, of course, to the same result. These occupation numbers are practically constant over the cycle. Therefore, ϵV is directly proportional to the transition probability $W_{\beta\delta}$.

Next, we consider the case that the b transition is on-resonance. The population transfer between the β and δ levels, caused by the weakly induced b transition, is calculated by a similar procedure.

However, the small additive term $-\epsilon$ appearing on the left-hand side of the second line of Eq. (2.21) is now included. Solving Eqs. (2.21), gives

$$\begin{aligned} n_\alpha &= 5/[12(1 - T_p)] - \epsilon/6T_p, \\ n_\beta &= 1 - 7/[12(1 - T_p)] - \epsilon/6T_p, \\ n_\gamma = n_\delta &= 1/[12(1 - T_p)] + \epsilon/6T_p, \end{aligned} \quad (2.22)$$

which yields for the difference $\Delta\bar{p}$ of the average polarization without and with the b transition at resonance

$$\Delta\bar{p} = \epsilon/3T_p. \quad (2.23)$$

At this point, it is crucial to analyze the phase coherence time of the system. Although the phase coherence is only partially lost over several modulation cycles, when spin-exchange collisions alone are effective $T_p < 2T_e$, the static and the rf magnetic fields are inhomogeneous enough to completely destroy the phase memory for successive b -transition pulses. Assuming, therefore, phase conservation only for the duration of one b -transition pulse, the familiar situation of a two-level system subjected to an rf field for a finite time T_p is encountered.⁸ According to Eq. (2.23) and the definition of ϵ , the line-shape analysis reduces then to a discussion of the transition probability $W_{\beta\delta}$ as a function of the applied frequency

$$W_{\beta\delta} = [(2b)^2/a^2] \sin^2(\frac{1}{2}aT_p), \quad (2.24)$$

where $a = [(\omega - \omega_0)^2 + (2b)^2]^{1/2}$, ω_0 is the resonance frequency, and $2b = \gamma H_1$ is the time-independent part of the matrix element of the rf perturbation.

The oscillating second factor in Eq. (2.24) has minima at $aT_p = 2n\pi$ and maxima at $aT_p = (2n+1)\pi$. The running index n is equal to $n = 0, 1, 2, \dots$. Equation (2.24) and Fig. 4 show that the relative intensities of the side maxima increase whereas the separations decrease with increasing rf power. The ratio of the first side maxima to the central maximum is 0.12 for optimum rf power.

For weak rf fields and $\omega \neq \omega_0$, the precession frequency a is given by $a = |\omega - \omega_0|$. One expects in this case maxima S_n in the line structure where the applied field satisfies $(\omega - \omega_0)T_p = (2n+1)\pi$. The relative intensity of subsequent side maxima is $S_0/S_n = [(2n+1)\pi^2]^{-1}$. For weak rf fields, the side fringes are relatively insensitive to inhomogeneities. An inhomogeneous field, which would already broaden the central fringe, smears out the side fringes to a much lesser extent, determined

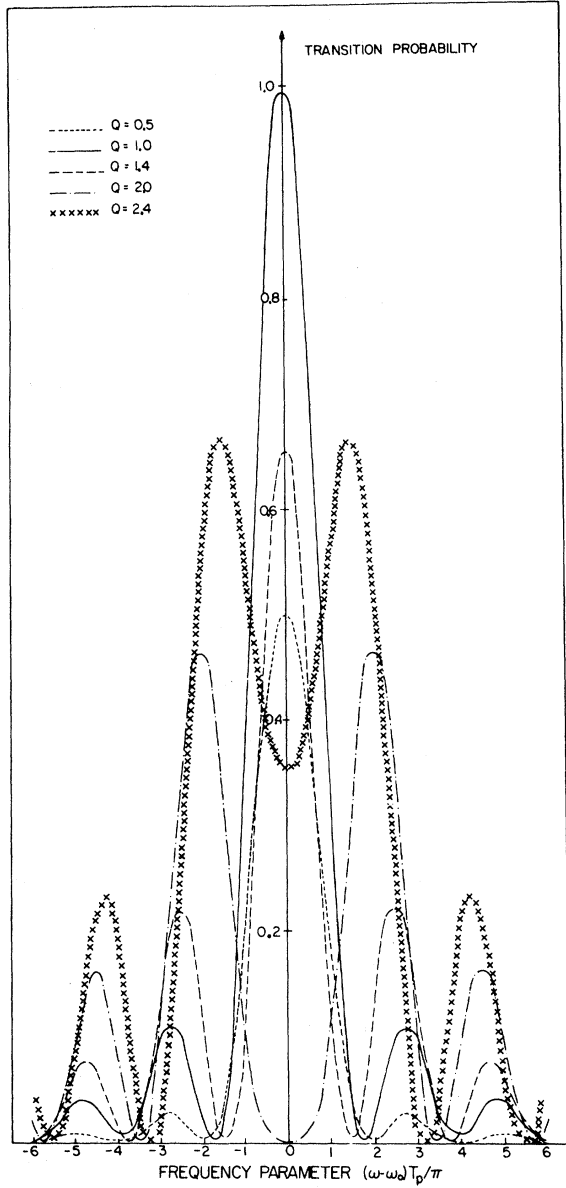


FIG. 4. Theoretical lines shapes for pulsed occupation numbers. The intensity is plotted against the parameter $|\omega - \omega_0|T_p/\pi$. The curves correspond to several different rf field strengths. The optimum signal is $Q=1$ with Q defined as $Q = \gamma H_1 T_p/\pi$.

by the ratio $\gamma H_1/n(\omega - \omega_0)$. This shows that even with fairly inhomogeneous weak H_1 fields, the side maxima should be resolved.

As a nonrigorous illustration of the previous discussion, the observed shape of the b -transition signal was compared to plots of $S^\dagger \beta \delta$ versus ν (see Fig. 19). The fitted curve represents the case of the optimum perturbation ($\gamma H_1 T_p = \pi$). Within the limits of the present signal-to-noise ratio, a

small structure of the proper size symmetric to the central maximum seems indicated. The first side maximum occurs, as expected, at $(\nu - \nu_0) = 3/2T_p = 19$ Hz.

The effects of charge exchange and other collisions limiting the ion lifetime have been neglected in the discussion, since these effects are not important when considering transition probabilities and line shapes.

In addition to the possible structure mentioned above, the line shape of the $\Delta F = \pm 1$ transitions, observed in the microwave region, revealed the occurrence of a first-order Doppler effect, (see Fig. 18). As a consequence of the periodic ion motion and the particular field configuration (see Sec. III, I) used, we have observed sidebands of the resonance frequencies of the hfs transitions at the various ion oscillation frequencies, including the Larmor precession frequency, of the ions in the external magnetic field. Occurrence of sidebands in the microwave spectrum of stored ions, caused by the modulation of the magnetic-resonance signal by the Doppler effect, will be discussed in another paper.

F. Electrodynamic Ion Storage

The containment of ${}^3\text{He}^+$ ions is achieved by means of an rf quadrupole cage, which, according to $(r_0/z_0)^2 = 2$, was constructed to be electrically symmetric. The curvature of the equipotential surfaces is chosen to produce a potential distribution having the familiar form⁹

$$\phi(r, z) = (U/4z_0^2)(r^2 - 2z^2), \quad (2.25)$$

with U referring to the applied voltages. Positive ions will be trapped along the z axis and lost in the r direction when a negative dc voltage $-U_0$ is applied to the ring electrode. When the dc voltage is replaced by a rf voltage, a pseudopotential ψ is generated, which, for an ion of mass m and charge e , may be expressed in terms of the time average of the squared electric field of amplitude E_0 as^{5,10}

$$\psi(\bar{r}, \bar{z}) = [e/4m\Omega^2] E_0^2(\bar{r}, \bar{z}), \quad (2.26)$$

where \bar{r} and \bar{z} are the coordinates of the guiding center, about which the forced micromotion of the ion with amplitude $\xi = \xi_0 \cos \Omega t$ occurs. Simultaneous application of dc and rf voltages generate an effective composite potential, ψ' being a superposition of a static dc potential and of a quasistatic pseudopotential

$$\psi' = \phi' + \psi. \quad (2.27)$$

Evaluating only the electric field generated by the rf voltage $U = V = V_0 \cos \Omega t$, we find from Eq.

(2.25),

$$E_0^2(\bar{r}, \bar{z}) = (V_0/2z_0^2)^2(\bar{r}^2 + 4\bar{z}^2), \quad (2.28)$$

which yields, together with Eq. (2.26),

$$\psi(\bar{r}, \bar{z}) = (\bar{D}_z/4z_0^2)(\bar{r}^2 + 4\bar{z}^2). \quad (2.29)$$

To characterize the binding of the ions to the weak-field region, \bar{D}_z is defined as the pseudo-potential well depth in the z direction, in analogy to an ideal harmonic potential. It holds

$$e\bar{D}_z = \frac{1}{2}m\bar{z}_0^2\bar{\omega}_z^2. \quad (2.30)$$

From the above equations, it can be shown that

$$\bar{D}_z = (V_0/2\sqrt{2})(\bar{\omega}_z/\Omega) = 2\bar{D}_r. \quad (2.31)$$

An additional dc bias field may easily be included in the discussion by superimposing the proper dc potential, derived from Eq. (2.25) on \bar{D}_z . This means that for the electrically symmetric trap construction used, half of the applied dc voltage has to be added to \bar{D}_r and half of the applied dc voltage has to be subtracted from \bar{D}_z . As an example, the potential well depths for the case that the ion macromotion is at resonance with the external detection circuit are listed below. According to the data in Table III and with the resonance of the ion motion occurring at half the negative sweep amplitude, the effective composite well depths become $\bar{D}_z = \bar{D}_z + 1.8 \text{ V} = 7.9 \text{ V}$ and $\bar{D}_r = \bar{D}_r - 1.8 \text{ V} = 1.25 \text{ V}$.

With reference to the definition of the coordinates of the guiding center, the complete motion of the z component, for example, may be described as

$$z(t) = \bar{z}(t) - \zeta_0 \cos \Omega t, \quad (2.32)$$

TABLE III. Typical experimental parameters for storage of ${}^3\text{He}^+$ ions.

axial dimension	z_0	= 25.5 mm
radial dimension	r_0	= 36.0 mm
dc bias	U_0	= 0 V
ac trapping amplitude	V_0	= 137 V peak
frequency of trapping rf	Ω	= $2\pi \times 1$ MHz
detection frequency	ω_0	= $2\pi \times 134$ kHz
axial oscillation frequency	$\bar{\omega}_z$	= $2\pi \times 123$ kHz
axial well depth	\bar{D}_z	= 6.1 V
radial well depth	\bar{D}_r	= 3.05 V
stored charge	q	= $8 \times 10^6 e$
electron current	i_e	= 10 mA
electron acceleration voltage	U_e	= 500 V
electron pulse duration	t_e	= 80 msec
coherent excitation amplitude	E_1	= 3 V
duration of excitation pulse	t_n	= 40 msec
excitation frequency	$\omega_0 + \Omega$	= $2\pi \times 134$ kHz
detection sweep amplitude	U_s	= -3.6 V
total detection sweep duration	t_s	= 32 msec
neutralization time	t_n	= 4 msec
capacity between end caps and ring electrode	C	= 34 pF
quality factor of detection circuit	Q_t	= 50
quality factor of stored ions	Q_i	= 100
ion storage time without Cs beam	T_i	= 25 sec
ion storage time with Cs beam	T_o	= 0.4 sec
${}^3\text{He}$ density	\bar{N}_{He}	= 2×10^8 atoms/cm ³
Cs density at site of trap	\bar{N}_{Cs}	= 1×10^8 atoms/cm ³
ultimate vacuum	p	= 1×10^{-10} Torr
ratio of ion-number signal to rms fluctuations of ion-number signal in presence of Cs beam at end of interaction interval (800 msec) comparing consecutive signals	S/N_f	= 400:1
ratio of ion-number signal to rms fluctuations without Cs beam	S/N_{f0}	= 2000:1
ratio of ion-number signal to rms thermal noise	S/N_t	= 8000:1

with $\xi_0 = eE_0(\bar{z})/m\Omega^2$. The above derivation implies that $(\bar{\omega}_z/\Omega) \ll 1$ and $\bar{z}(t)$ is given by $\bar{z} = \bar{z}_0 \cos \bar{\omega}_z t$. The complete motion is then a superposition of the guiding center macromotion at $\bar{\omega}_z$ and of the micro-motion at Ω .

Using Eqs. (2.21) and (2.28), Eq. (2.32) finally becomes

$$z(t) = \bar{z}_0 (1 - \kappa \cos \Omega t) \cos \bar{\omega}_z t, \quad (2.33)$$

where $\kappa = \sqrt{2} (\bar{\omega}_z/\Omega)$.

It should be noted from Eq. (2.33) that the pseudopotential approach yields a strong carrier frequency at $\bar{\omega}_z$ together with sideband frequencies at $\Omega + \bar{\omega}_z$. The rigorous solution of the ion motion gives, in addition, higher spectral components at $n\Omega + \bar{\omega}_z$, where n takes the values $n = 2, 3, 4, \dots$.

The following shows in summarized form the rigorous treatment including, at the same time, the effect of an additional static magnetic field. When the magnetic field is produced parallel to the z direction the z motion is not influenced; however, the motion in the xy plane is modified. It is usual to choose for the calculation a frame of reference in which the equations of motion take a simple form. In the transformed form, the motion may be described by

$$\begin{aligned} d^2x/d\xi^2 + (a_x + 2q_x \cos 2\xi)x &= +2\omega'_L dy/d\xi, \\ d^2y/d\xi^2 + (a_y + 2q_y \cos 2\xi)y &= -2\omega'_L dx/d\xi, \end{aligned} \quad (2.34)$$

$$d^2z/d\xi^2 - 2(a_z - 2q_z \cos 2\xi)z = 0,$$

where $\xi = \frac{1}{2}\Omega t$,

$$a_x = a_y = a_r = 4eU_0/mr_0^2\Omega^2,$$

$$q_x = q_y = q_r = 2eV_0/mr_0^2\Omega^2,$$

$$\omega'_L = eH/m\Omega.$$

The symbol ω'_L refers to the Larmor precession in the transformed time ξ . When considered in a coordinate frame, which rotates about the z axis at ω'_L , the motion of the stored ions admits a transparent geometrical description. The rotating frame (u, v, z') is connected with the fixed laboratory frame (x, y, z) by the transformation

$$\begin{pmatrix} u \\ v \end{pmatrix} = \begin{pmatrix} \cos \omega'_L \xi & -\sin \omega'_L \xi \\ \sin \omega'_L \xi & \cos \omega'_L \xi \end{pmatrix} \begin{pmatrix} x \\ y \end{pmatrix} \quad (2.35)$$

Since the z axis is the same in both reference sys-

tems, it is sufficient to consider only the transformation of the xy plane into the uv plane. Using the following identities

$$\begin{aligned} r_+ &= u + iv = (x + iy) \exp(i\omega'_L \xi), \\ r_- &= u - iv = (x - iy) \exp(-i\omega'_L \xi), \end{aligned} \quad (2.36)$$

the x and y motions in Eq. (2.34) are decoupled and give

$$d^2r_{\pm}/d\xi^2 + (a'_r + 2q_r \cos 2\xi)r_{\pm} = 0, \quad (2.37)$$

with $a'_r = a_r + (2\omega'_L/\Omega)^2$ and $\omega'_L = eH/2m$ being the Larmor frequency in the usual time. The result of Eq. (2.37) is a consequence of Larmor's theorem, that the motion of a charged particle in a weak magnetic field consists of the solution without a field, on which an added rotation at ω'_L about the axis of the field is superimposed.

The small modification of the ion motion by the external magnetic field is of little interest as far as ion storage properties are concerned. However, the microwave absorption is modified by the occurrence of Doppler sidebands, which are about $\pm\omega'_L$ distant from the microwave transition frequencies.

III APPARATUS

A. Vacuum System

Figure 5 shows schematically the over-all arrangement of the basic parts of the apparatus, including the vacuum chamber. To prevent the background gas from limiting the ion lifetime, the collision rate between ${}^3\text{He}^+$ and the rest gas atoms has to be smaller than the collision rate between ${}^3\text{He}^+$ and the cesium atoms of the beam. Under typical conditions of the experiment, the beam density at the site of the trap was about 2×10^{-8} Torr which requires an even lower residual gas pressure. An ultimate pressure of 10^{-10} Torr was achieved by using a 500 liter/sec vacuum pump and by constructing the major parts of the vacuum system of pyrex glass. Initially the system was baked at temperatures up to 400°C and pumped by a mercury diffusion pump which was sealed off after a pressure of 10^{-6} Torr had been reached. The vacuum pump was connected with the vacuum chamber by a stainless-steel tubing of 250 cm in length. In this way, inhomogeneous stray fields of the pump magnets, arranged as a quadrupole, were kept below a critical level. The conductance of the tubing was 10 liter/sec, which is comparable to about half the pumping speed for He. The purpose of the lower conductance was to minimize the effects of undesirable fluctuations in the pumping speed. Turning on the electron gun raised the

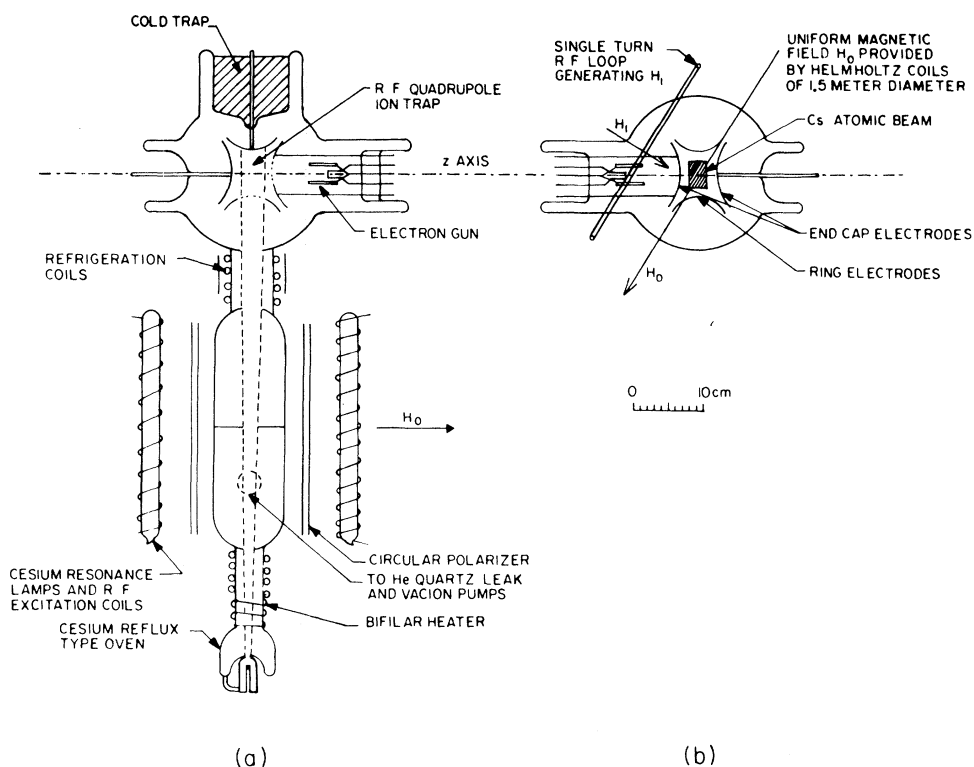


FIG. 5. Diagram of the apparatus designed to determine the hfs of ${}^3\text{He}^+$. (a) Front view of the apparatus. The glass vacuum chamber containing the ion trap and the Cs atomic beam are depicted. The axis of the trap was actually rotated 45° out of the plane of the drawing. The optical pumping arrangement for polarizing the Cs atoms is also indicated. (b) Apparatus seen from top. Since the microwave field is practically parallel to the z axis, both σ and π transitions were induced in the same geometry. The low-frequency transitions were excited by a rf field H_1 perpendicular to H_0 .

pressure to 5×10^{-10} Torr. A cold trap on top of the electrode structure could be filled with dry ice to suppress back-scattered unpolarized cesium atoms. The ${}^3\text{He}$ gas was admitted continuously through an electrically heated quartz leak, which was isolated against room-temperature fluctuations and filled with 110 Torr of ${}^3\text{He}$. The enriched isotope sample, containing 99.6% ${}^3\text{He}$ and 0.4% ${}^4\text{He}$ was obtained from the U.S. Atomic Energy Commission. Adjusting the temperature of the leak ensured an equilibrium ${}^3\text{He}$ pressure of about 2×10^{-8} Torr. The approximate ${}^3\text{He}$ pressure was derived from the indication of a Bayard-Alpert-type ionization gauge (Varian UHV - 12P).

B. Ion Storage

The ion storage device consists of three electrodes between which a three-dimensional symmetric quadrupole field is produced. The central ring electrode is a hyperboloid of revolution, symmetric about the z axis. Having the same asymptote cones, the two end cap electrodes form complementary hyperboloids. The radius of the quad-

rupole electrode in the center is $r_0 = 36$ mm. All electrodes were accurately spun from pure grade aluminum and were highly polished. The surface was not coated with a gold film as in the preceding experiment.⁴ There was experimental evidence for the forming of an Au-Cs compound, which roughened the surface and also decreased the conductivity. Although for constructional reasons the electrodes are truncated in an outer region, the quadrupole field distribution is not significantly affected. The ${}^3\text{He}^+$ ions are formed by bombarding the residual ${}^3\text{He}$ gas with a beam of electrons. The electron gun assembly consists of an indirectly heated commercial cathode, Philips Type "L", and a Wehnelt cylinder. The experimental problem not to distort the external static magnetic field was circumvented by supplying the heater with an rf current from an oscillator near 4 MHz. The Wehnelt cylinder served to confine the electron beam to the vicinity of a perforated area of 12 mm radius in the center of one end cap electrode. The Wehnelt cylinder was maintained at a constant potential of -300 V with respect to the dc grounded trap. In order to pulse the electron beam on, the potential of the

better than 1%, even though the electron beam absorbed energy, when it was pulsed on. To achieve optimum trapping conditions for ions of different masses, the rf amplitude could be adjusted to any fixed value between 50 and 300 V. At the same time, provisions were made to vary a small additional dc bias voltage between positive and negative values of a few volts. The trapping potentials for maximum ${}^3\text{He}^+$ signal were 137-V peak at 1 MHz and zero dc voltage. This corresponds to an asymmetric operation of the trap, the potential well depths in the z and r directions being $\bar{D}_z = 6.1$ V and $\bar{D}_r = 3.05$ V.

A new ion detection system was developed to monitor the ion number. It is based on the coherent excitation of the ion motion at $\omega_0 = \bar{\omega}_z$ by a homogeneous rf field at the sideband frequency $\Omega + \omega_0$. An analysis of the coherent ion motion excitation mechanism is given in Sec. IV A. The excitation voltage applied at one end cap across a tuned LC circuit, is pulsed on together with the ion detection sweep. The duration and strength of the pulse are adjusted for maximum ion motion signal. Care was taken that the source impedance at ω_0 and Ω was practically negligible to avoid direct coupling to the detection tank circuit, tuned to the fundamental ion macromotion $\bar{\omega}_z = \omega_0$. The excitation voltage was low enough not to disturb the ion motion at frequencies other than $\Omega + \bar{\omega}_z$. The detection is effected in a LC parallel circuit resonant at ω_0 with a quality factor $Q = 60$. The split-tank circuit design chosen has advantages over the conventional resonant step-down transformer-transmission line-resonant step-up transformer approach. The circuit is simple and uncritical, since the drive frequency Ω is strongly rejected, and only one tuned circuit contributes thermal noise. The latter property may also be expressed by saying that the circuit has a high filling factor, i. e., the electric field energy stored in the resonant circuit is mostly concentrated inside the ion cage where it may interact with the ions.

At the low-impedance point a high-impedance coil establishes a dc return path for the ionizing electron current and also holds the two end caps at the same dc potential. An additional series resonant LC circuit grounds the detection electrode with respect to the trapping voltage at Ω .

For detection the ion frequency $\bar{\omega}_z$ was varied through the fixed resonance frequency ω_0 of the detection circuit by linearly sweeping the dc voltage. After narrow banded amplification the ion number signal could be displayed on a scope. Typical operating parameters of the ion trap are summarized in Table III.

F. Microwave Generation and Stabilization

Care was taken to secure a stability of at least 1 part in 10^9 for all applied microwave fre-

quencies over a period of several hours. The stability for the field-independent b transition which, of course, was of primary experimental interest, was better than 1 part in 10^{10} . The microwave generation and stabilization system is shown in Fig. 7. The microwave signals necessary were derived from a General Radio secondary frequency standard, model 115B, which was constantly monitored by a Hewlett-Packard low frequency comparator, type 117 A-VFL, against the National Bureau of Standards (NBS) low-frequency station WWVB at 60 kHz. The frequency standard controlled a Hewlett-Packard 5100A frequency synthesizer, operating near $\Delta\nu/176 = 49\,236\,777$ Hz.

The microwave power for the field-independent b transition was produced by straightforward multiplication of the synthesizer signal using two step recovery diode multipliers and a Boonton 320A tuned amplifier. The microwave power could be attenuated by 20 db for the purpose of lowering the strength of the hfs transition field in the cavity well below the point of power broadening.

Because of the residual field inhomogeneities of the external magnetic field, the power for the field-dependent a - or c -microwave transitions had to be larger by more than four orders of magnitude than for the b transition. A Varian reflex klystron, type X 13B, was used to supply about 100 mW near 8.6 GHz. A Dymec klystron synchronizer, model 2650A, eliminated long-term drifts and incidental frequency fluctuations by phase locking the klystron to an internal crystal oscillator, the crystal being oven mounted for temperature stabilization.

Two different internal crystals had to be used, to synchronize either the a - or the c -microwave field. The frequency of the internal crystal was chosen at such a frequency around 100 MHz that an if-frequency near 30 MHz was obtained, when a harmonic of the crystal frequency was mixed with a small fraction of the klystron power. The 84th harmonic of a crystal cut to 103.4005 MHz for the a -transition field was used, and the 86th harmonic of a crystal resonant at 101.2273 MHz was used for the c -transition field.

However, to achieve the desired stability of the signal, it was still necessary to further control the internal crystal oscillator. This was achieved by phase locking the difference frequency of the corresponding harmonic of the proper internal crystal near 100 MHz and the very stable b -transition frequency, to a second voltage tunable crystal oscillator at a lower frequency near 10 MHz. At 10 MHz the stability requirements were less stringent. Nevertheless, much attention was given to carefully select a well-suited oscillator and to operate it properly. A short-term stability of one part in 10^8 is satisfactory, as the reference frequency near 10 MHz is only about 1% of the total

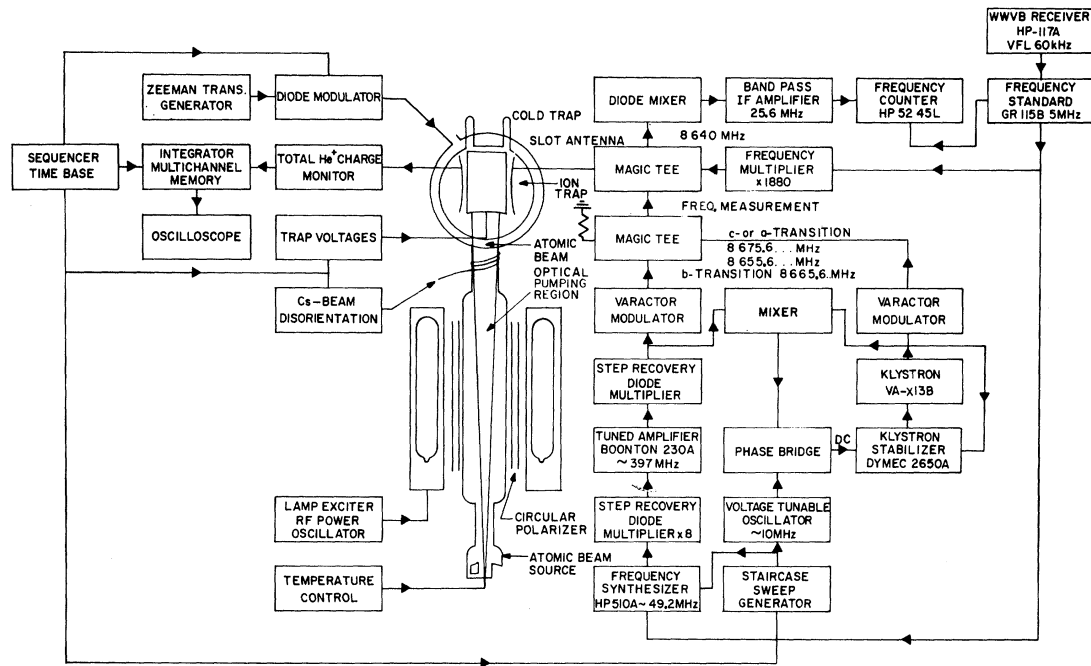


FIG. 7. Over-all block diagram of the $^3\text{He}^+$ experiment.

microwave hfs transition frequency. In a phase bridge, a regulation voltage was produced and then applied to the voltage tunable if reference of the Dymec synchronizer.

In order to observe the field-dependent a or c transitions, the klystron frequency has to be varied through resonance. This was achieved by linearly sweeping the voltage tunable 10-MHz oscillator.

When the field-independent b transition was induced, the synthesizer frequency was continuously varied over a sweep range of about 0.3 Hz. At the same time, the crystal stabilized Zeeman transition generator and the klystron frequency were kept constant at the d - and c -transition frequency, respectively. To achieve a constant microwave c frequency, a small correction voltage corresponding to the synthesizer sweep was applied to the voltage tunable reference oscillator.

G. Spectral Purity

It is well known that when multiplying a frequency broad banded, the ratio of the total sideband over to the signal power increases as the square of the multiplying factor. We therefore checked our multiplying system to determine whether it yields a narrow spectrum of high spectral purity, which is essential for the precise measurement of the microwave b transition.

To ensure that the spurious content was well below an acceptable level, the system shown in Fig. 8 was used. In this arrangement, the transition

frequency is frequency modulated by a sawtooth generator, which also supplies the horizontal sweep voltage on the oscilloscope. The reference frequency results from multiplying the frequency of the local oscillator of an atomicron (Model NC 1001A), in which the Cs beam stabilization was, however, inactive. The beat note after the first mixer was converted to the audio range by a second mixer. After passing a narrow band filter at a center frequency of 2 kHz, noise spectrum plots were produced on an oscilloscope. It was possible to achieve a minimum filter bandwidth of 1 Hz, measured at the 6-dB points by means of a Q-multiplier circuit. The spectrum in Fig. 9(a) shows a

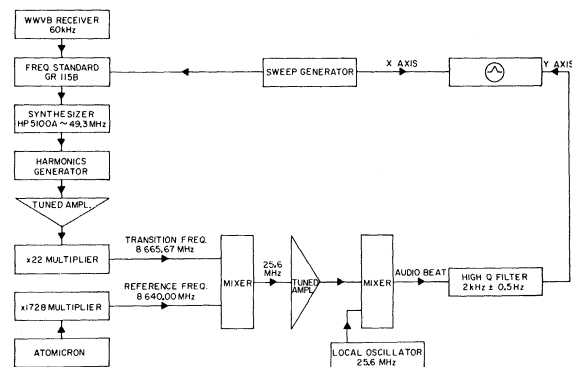


FIG. 8. Block diagram of apparatus used for spectrum analysis.

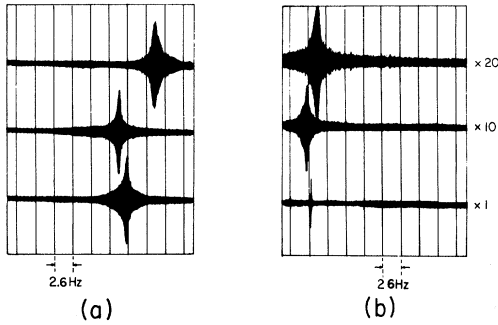


FIG. 9. Spectrum of 2 kHz beatnote of two microwave signals near 8.6 GHz. (a) The horizontal display is 2.6 Hz per division with the higher Q filter employed. (b) The horizontal display is 26 Hz per division with the lower Q filter employed. The amplification increases from the bottom trace to the middle trace by a factor of 10, and from the bottom trace to the top trace by a factor of 20. The amplified traces indicate small sidebands at 60 and 120 Hz.

width of about 1 Hz confirming that the width of the power spectrum is, at most, equal but probably less than the resolution of 1 Hz. The spectral purity in a wider range is investigated in Fig. 9(b). The display shows that with each of the two microwave sources used, the power in the 60- and 120-Hz sidebands was more than 30 db below the center frequency power.

H. Frequency Measurement

A heterodyne method was used to measure the various frequency points of a single resonance passage of the b transition to about 0.1 Hz. To avoid excessively long counting times, this method was chosen over another possible, more direct, way of frequency determination, in which the output of the last variable 0.1 Hz decade of the frequency synthesizer may be counted for a fixed accurately determined time. A resolution of 0.1 Hz at the microwave frequency was achieved in 10 sec with the heterodyne conversion technique, whereas, the direct counting method would need some 1000 sec of counter gating time to yield the same accuracy.

Figure 10 shows a block diagram of the frequency measuring system. A multiplier chain with a total multiplying factor of 1728 produces a reference frequency at 8640 MHz from the 5-MHz General Radio frequency standard. This local standard had a predictable low-drift rate, typically several parts in 10^{11} over a day, so that a continuous phase comparison with the 60-kHz signal of the NBS station WWVB could be effected by means of a Hewlett-Packard 117A-VLF comparator. The applied microwave b -transition frequen-

cy was then mixed with the reference frequency to produce a beat frequency near 25.6 MHz. After amplification, this difference frequency was counted with a Hewlett-Packard frequency counter, type 5245L, which in turn was phase locked to the local frequency standard. By simply adding the frequency counted to the reference frequency, the applied transition frequency was evaluated. In a single resonance run for the b transition, the applied frequencies corresponding to the various channels were measured before and after observation of the induced transitions.

In addition, the double quantum frequency ν_z was measured alternately by directly counting the applied low frequency at the various points of the double quantum signal. The correction δ necessary for the evaluation of the zero-field hfs splitting $\Delta\nu$ could then be obtained from Eq. (2.3).

I. Microwave Field Geometry

To effectively induce hfs transitions in the cm wavelength region, a well-defined rf field of proper spatial distribution has to be applied. A trap design, that makes use of the properties of a cavity resonator, is shown in Fig. 11. The most suited cavity modes in a three-electrode arrangement, which still preserves the trapping features while exciting strong microwave fields in the center, are modes closely resembling the cylindrical TE_{01n} modes. In such a mode, only azimuthal wall currents are present and no currents flow across the corners of the cylinder. Even without a connection between the electrodes it is possible to achieve sufficient rf field strengths and additionally, at the same time, to suppress the unwanted degenerate TM_{11n} modes. According to the particular size of the ion trap an excitation of the TE_{013} mode was chosen.

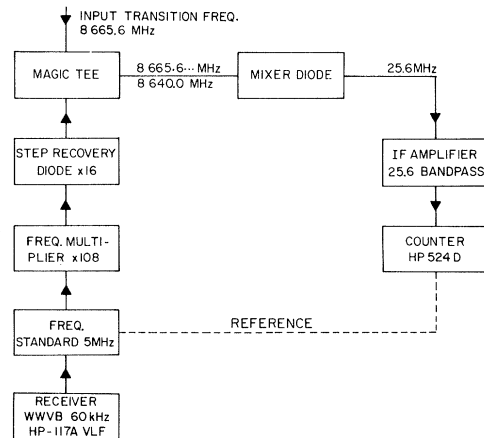


FIG. 10. Block diagram of the microwave measuring circuit used to determine the b -transition frequency.

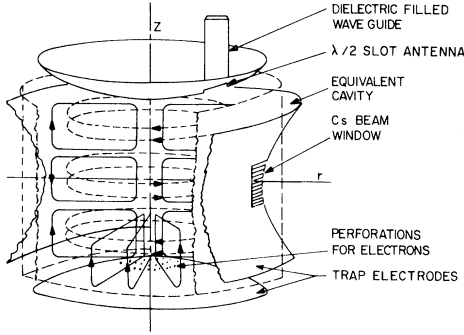


FIG. 11. Microwave field in trap showing, schematically, the TE_{013} mode. Solid lines represent the magnetic field and broken lines are the electric field. The equivalent right angular is also shown.

The standard theory for the electric properties of right circular cylindrical cavities may be applied in first approximation to the present situation by substituting equivalent cylindrical surfaces instead of the rotationally symmetric hyperbolic surfaces. In a test setup, we have experimentally established the position of such equivalent cylindrical surfaces. For the trap structure used and a resonance frequency near 8.6 GHz, the positions were found to be located at a distance of $0.4h$ behind the apex of the hyperboloids, with h being defined as $h_z = Z_0 - z_0$, $h_r = R_0 - r_0$. Here Z_0 , R_0 defines the smallest cylinder containing the actual trap structure.

Microwave power was fed into the trap by means of a $\frac{1}{2}\lambda$ slot antenna cut into one end cap electrode. A Teflon-filled waveguide was butted through a re-entrant glass tube against the narrow slot. The cavity quality factor Q was appreciably affected by the slot and also by the atomic beam window cut into the central ring electrode. A trap structure Q between 200 and 300 was aimed at in order to produce a sufficiently high microwave field strength and to avoid, at the same time, tuning adjustments for the various transition frequencies near 8.6 GHz spread over a range of 20 MHz. By rotating the trap and, thereby, the cavity axis, 45° against the H_0 field, it was possible to induce both π and σ transitions by the same microwave field geometry.

IV. MANIPULATION OF STORED CHARGE

A. Excitation of Coherent Ion Motion

The discussion concerns the oscillation of the center of charge of an ensemble of ions in a three-dimensional potential well under the influence of rf fields, which are resonant with different motional frequencies of the ions. Figure 12 shows

in a cross section of the quadrupole ion trap the application of the different alternating electric fields used to manipulate the stored charge.

It is known that ion oscillations can be excited by a homogeneous rf field at $\bar{\omega}_z$ using the absorption method, in which case motional resonance may be detected by the damping of the driving carrier at ω_0 when $\bar{\omega}_z = \omega_0$.

In the present experiment, we have developed a different emission method in which excitation by a homogeneous rf field at a sideband frequency $n\Omega \pm \bar{\omega}_z$ is used. Such a coherent excitation can, according to Eq. (2.33), be expected to occur. Of all sideband frequencies, we have chosen to use the first sideband frequency at $\Omega + \bar{\omega}_z$, because the ion motion, having its dominant component at $\bar{\omega}_z$ can be most effectively excited by a homogeneous rf field $E_1 \cos(\Omega \pm \bar{\omega}_z)t$. Such a sideband excitation is very useful when detecting the stored charge by a circuit tuned to $\omega_0 = \bar{\omega}_z$, because it completely eliminates a troublesome large amplitude carrier, which is present in the previously used absorption method.

In our discussion we use the pseudopotential approach of Eq. (2.26),

$$\bar{F}(\bar{z}) \propto \partial \psi / \partial \bar{z} \propto \partial \langle E_z^2 \rangle_{\text{av}} / \partial \bar{z}.$$

For E_z we take

$$E_z = (E_m \bar{z} / z_0) \cos \Omega t + E_1 \cos(\Omega \pm \bar{\omega}_z)t,$$

where E_m is the amplitude of the field on the elec-

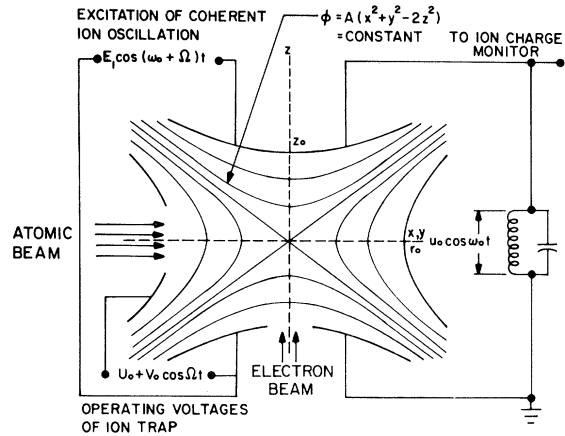


FIG. 12. Cross section of the quadrupole ion trap showing, schematically, the electric potential distribution of the trapping voltage, $U_0 + V_0 \cos \Omega t$. The atomic beam and the electron windows are indicated. The voltage $u_0 \cos \omega_0 t$ is induced in the resonant circuit by the cooperative motion of the ions and allows their detection. The ion oscillation is excited by a homogeneous alternating field at $\Omega + \omega_0$.

trode $x=y=0$. Averaging over one period $2\pi/\Omega$, it follows

$$\langle E_z^2 \rangle_{\text{av}} = E_m^2 \bar{z}^2 / (2z_0^2) + \frac{1}{2} E_1^2 + (2\bar{z} E_1 E_m / z_0) \times \langle \cos^2 \Omega t \cos \bar{\omega}_z t \mp \cos \Omega t \sin \Omega t \sin \bar{\omega}_z t \rangle_{\text{av}}. \quad (4.1)$$

Carrying out the average over the last term taking $\sin \bar{\omega}_z t$, $\cos \bar{\omega}_z t$, as quasiconstant, gives finally after differentiation with Eqs. (2.28)-(2.31)

$$-(1/e) \bar{F}(\bar{z}) = (\bar{z} E_m / z_0 + E_1 \cos \bar{\omega}_z t) \bar{\omega}_z / (\Omega 2\sqrt{2}). \quad (4.2)$$

Here the first term is the restoring force due to the trapping field at Ω , while the second term demonstrates that an excitation at $\bar{\omega}_z$ takes place. Except for the amplitude reduction by $\bar{\omega}_z / (\Omega 2\sqrt{2})$, this case is completely equivalent to the familiar direct sinusoidal excitation at $\bar{\omega}_z$.

As far as the noise contributions resulting from small fluctuations of the excitation voltage are concerned, an emission technique employing excitation at $\Omega + \bar{\omega}_z$ has certain advantages over the conventional absorption method, employing excitation at $\bar{\omega}_z$. In the absorption method, instabilities of the total large excitation voltage add directly to the small absorption signal. On the other hand, analogous noise in the emission signal resulting from sideband excitation is only proportional to fluctuations in the excitation voltage at $\Omega + \omega_z$, which makes the voltage stability requirements much less stringent.

B. Detection of the Ion Number Signal

The method of charge detection shall be treated explicitly to make a quantitative estimate of the size of the ion number signal and of the background noise, which might be expected.

First, an expression for the absolute signal size is derived. The simple case of a charged particle, oscillating perpendicularly between the parallel plates of a capacitor connected to a voltage u_0 , is a reasonable approximation for the motion of the ion in the trap. The separation of the parallel plates is $2z_0$. We shall consider the situation during a short time interval Δt , during which the velocity v of the charge q may be considered as being constant. Then, the moving charge experiences a force

$$F(t) = Eq = qu_0 / 2z_0, \quad (4.3)$$

and energy is transferred from the ion motion into electric energy by inducing an induction current into the external circuit, connecting the two elec-

trodes. Because of energy conservation, we may write

$$(U_0 / 2z_0) qv \Delta t = u_0 i_i \Delta t, \quad (4.4)$$

and hence $i_i = (q/2z_0) dz/dt$. This induced current seems to come from a high-impedance current source.

Since the motion of the charge is harmonic at $\bar{\omega}_z$, it is possible to develop a high voltage across the current source by paralleling C by an inductance L , which fulfills the resonance condition of $\bar{\omega}_z^2 LC = 1$. In steady-state situations, the current source then simply appears to be paralleled by the shunt impedance of the tuned circuit R_s , across which it develops a peak signal voltage of amplitude

$$u_0 = R_s q \bar{z}_0 \bar{\omega}_z / (2z_0), \quad (4.6)$$

with \bar{z}_0 being, according to Eq. (2.32), the peak amplitude of the guiding center motion.

However, in the situation realized in the ion trap, more than one ion is present. It is necessary to consider that the energy of the oscillation of the center of mass of the ion cloud, once excited, will decay and be degraded to disordered motion. The coherent oscillation will decay approximately exponentially with a characteristic phase memory time $t_d = Q_i / \bar{\omega}_z$, due to various causes, such as imperfections of the trap, ion-ion interactions, collisions with residual gas atoms, etc.

In this experiment, a relative linewidth $\Delta \bar{\omega}_z / \bar{\omega}_z = Q_i^{-1}$ of the ion number signal of about 1% was realized. To obtain, under these circumstances, a strong response reflecting the absolute magnitude of q as closely as possible and side effects due to variable line shape, anharmonicity, and charge-dependent deformation of the potential well, etc., as little as possible, it appears advantageous to subject the ion cloud to a short square rf pulse at any one of the ion motion frequencies at $n\Omega + \bar{\omega}_z$ ($n=0, 1, 2, \dots$). We have used mainly the first sideband frequency at $\Omega + \bar{\omega}_z$. The pulse was made intense enough to drive the center of mass of the ion cloud against the electrodes at $\pm z_0$ in a time $t_n \ll Q_i / \bar{\omega}_z$, effecting complete neutralization of the ion cloud.

Assuming that the ion cloud is concentrated in a region which is small compared to z_0 the forced ion motion is accompanied by an rf current pulse of triangular envelope, duration t_n , and maximum amplitude $\frac{1}{2} q \bar{\omega}_z$.

The response of the tuned circuit depends strongly on its Q value Q_t . For $Q_t \ll t_n \bar{\omega}_z$, the signal voltage u_0 faithfully follows the current pulse assuming a maximum value $u_0 f = \frac{1}{2} R_s q \bar{\omega}_z$ which we were interested to derive. It is now possible to obtain, for instance, the absolute value of q from

the peak value (other methods to derive q are given in Sec. IV C). Furthermore, it is evident that the bandwidth of the detection apparatus must be made wider as t_n decreases, admitting more and more thermal noise while the peak signal u_{0f} remains constant.

Next, the optimum signal-to-noise conditions of an ion-storage experiment are analyzed using an energy approach. The trapping voltages have been adjusted to yield $\bar{D}_r = \bar{D}_z = \bar{D}$. Since only the situation during the period of the detection pulse has to be considered, we assume that a constant resonant drive excites a c. m. oscillation of energy

$$\bar{W}_c \ll ne\bar{D} \quad (4.7)$$

of the ion cloud in the trap. However, the coherent energy \bar{W}_c , which is maintained at an equilibrium by the rf drive, is continuously degraded to incoherent energy \bar{W}_i of the ion cloud at a rate

$$d\bar{W}_i/dt = \bar{W}_c/t_d \quad (4.8)$$

Mostly due to the increase in incoherent energy, the ions will finally hit the electrodes, where they are lost after the neutralization time t_n ($t_n \gg t_d$). At that moment, the total ion energy \bar{W} is, according to condition (4.7), practically

$$\bar{W} = \bar{W}_i = ne\bar{D}. \quad (4.9)$$

Integration of Eq. (4.8) yields with Eq. (4.9)

$$\bar{W}_c = (ne\bar{D})t_d/t_n. \quad (4.10)$$

The coherent as well as the incoherent ion cloud oscillation induces coherent and incoherent oscillations in the tuned detection circuit of energy W_{tc} and W_{ti} , with $W_{ti} \ll W_{tc}$. It follows

$$W_{tc} = n\bar{W}_c t_0/t_{zt}, \quad (4.11)$$

where $t_{t0} = Q_t/\omega_z$ and $t_{zt} = mz_0^2/q^2R_s$ stands for the characteristic single-ion z -motion damping time due to energy loss in the real impedance of the tuned LC circuit. The induced incoherent energy at the moment when the ions are lost at the electrodes is

$$W_{ti} = ne\bar{D}t_0/t_{zt}, \quad (4.12)$$

comparing Eqs. (4.11) and (4.12) and using Eq. (4.10), it follows that the incoherent energy contribution to the coherent signal is negligible for typical ion numbers ($n \approx 10^6$) used in ion-storage experiments.

Denoting, therefore, the signal voltage by S and the rms noise voltage by N , both averaged over the observation interval t_m chosen equal to t_n , we have $S^2 \propto W_t$ and $N^2 \propto kTt_0/t_n$. For the optimum signal-to-noise ratio we find

$$(\underline{S}/\underline{N})^2 = n^2 e \bar{D} t_d / k T t_{zt}. \quad (4.13)$$

The following signal behavior underlies Eq. (4.13). The optimum signal-to-noise ratio is independent of the choice of t_m , provided $t_n \gg t_d$, t_{t0} . When the amplitude of the resonant excitation pulse is increased, the average signal amplitude \underline{S} increases at first while the optimum observation interval $t_m = t_n$ decreases, resulting in larger noise \underline{N} in such a way that $\underline{S}/\underline{N}$ remains constant. Later, when the condition $t_n \gg t_d$, t_{t0} is beginning to be violated, t_m approaches the minimum value t_{t0} , the persistence time of the signal in the tuned circuit induced by the ions, and \underline{N} becomes constant. Simultaneously, \underline{S} goes through a maximum and then decreases rapidly as the shorter and shorter ion current pulses of constant peak amplitude excite the tuned circuit less and less and $\underline{S}/\underline{N}$ deteriorates.

Using the expressions for $e\bar{D}$ and t_{zt} , Eq. (4.13) may be rewritten

$$(\underline{S}/\underline{N})^2 = n^2 e^2 Q_i Q_t / 8kTC. \quad (4.14)$$

In the actual experiment, the ions have not been subjected to a constant frequency resonant excitation pulse as assumed in the analysis. Their resonance frequency $\bar{\omega}_z$ has rather been swept through the effective force field at ω_0 of an applied excitation field at $\Omega + \omega_0$. Assuming that the traversal is quasistationary and that during its course the ions are driven against the electrodes, we take here for t_m the distance between half-maximum points of the observed response pattern on a time scale, i. e., the dwell time in the resonance line. A typical ion-number signal is shown in Fig. 13.

The whole question of tuned circuit noise now denoted by \underline{N}_t , becomes important in our experiments only when the tuned circuit noise is larger than the ion noise \underline{N}_i , associated with the Poisson fluctuations \sqrt{n} in the ion number n . Good design should aim for

$$n_m = 8kTC / (e^2 Q_i Q_t) \ll n. \quad (4.15)$$

Here n_m is the critical ion number for which Poisson fluctuations equal those due to thermal noise. If this condition is satisfied, the observed signal-to-noise ratio will essentially be

$$\underline{S}_i / \underline{N}_i = \sqrt{n}. \quad (4.16)$$

In Figs. 14(a) and 14(b), oscilloscope traces of

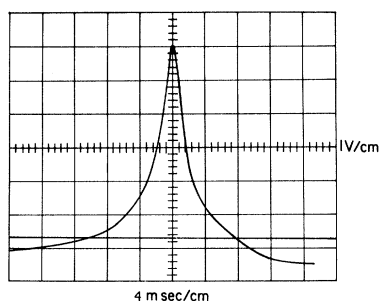


FIG. 13. Rectified ion-number signal. The ion macro-motion is coherently excited with a frequency at $\Omega + \omega_0$ and the voltage induced in a fixed circuit tuned to ω_0 is observed, when simultaneously sweeping the ion macro-motion frequency through resonance. The rectified signal voltage was biased with -1.35 V at the diode output by a mercury cell. The straight line represents zero dc voltage. Since the analog to digital converter is only sensitive to positive voltages, system noise outside the ion-number signal is prevented from being integrated. Sweeping from right to left, the total sweep length was 40 msec.

an unrectified ion-number signal and of the thermal noise level are shown. The ion-number signal was obtained by coherently exciting the ion macro-motion and by observing the voltage induced in a fixed tuned circuit, when sweeping the ion macro-motion frequency through resonance.

However, even without external excitation of the ion motion, an ion signal could be registered. Such an ion signal, reflecting the disordered motion of the stored ion cloud, is shown in Fig. 15. In the present experiment, it was not practical to fully analyze these data. The order of magnitude of the related equivalent average ion temperature in our present trap may, however, be estimated, by deriving it from the well depth of the rf pseudopotential, $3kT \lesssim e\bar{D}_{\min}$. Taking $\bar{D}_{\min} = 3.05$ V from Table III one finds $T_i \lesssim 23\,000^\circ\text{K}$.

To illustrate the previous discussion, a comparison of the observed signal-to-noise ratio with the expected signal-to-noise ratio shall be made. For this comparison, the ion number needs to be known. We only quote here that about 8×10^6 ions were stored with a lifetime of 20 sec. The measurement of the ion charge will be discussed in Sec. IV C.

With no Cs beam present, the measured signal-to-noise ratio, when comparing two consecutive signals, was 2000:1, showing that the noise is to a substantial part due to statistical ion-number fluctuations. When comparing the ion-number signal with the thermal noise, a ratio of 8000:1 was found. Using the above ion number and the relevant circuit values $C = 50$ pf, $Q_f = 60$, and $Q_i = 100$, Eq. (4.14) gives $(\underline{S}/\underline{N})_{\text{theoret}} = 6 \times 10^4$.

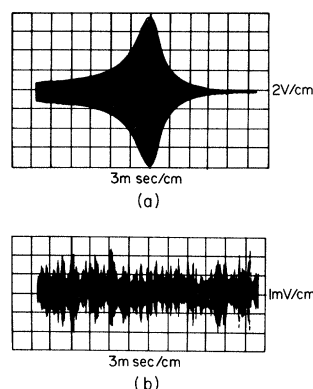


FIG. 14. Oscilloscope traces. (a) Ion-number signal. After coherent excitation of the ion macro-motion at the sideband frequency $\Omega + \omega_0$, the voltage induced in a fixed tuned circuit is observed when sweeping the macro-motion frequency through resonance. The Cs beam was turned off for this measurement. Experimental parameters: $V_0 = 137$ peak, $U_0 = 0$ V, $U_S = -2.5$ V, $i_e = 25$ mA, $T_e = 20$ msec, sensitivity 2 V/cm, amplification 2000. (b) Total system noise. The electron gun is turned off so that no ions are created. There was practically no change in noise amplitude with the trapping rf switched off or the detection input grounded, showing that mainly thermal noise was observed. Sensitivity 1 mV/cm, amplification 2000. In both oscilloscope traces the time increases from left to right. The linear sweep period was 32 msec.

This value agrees reasonably well with the one observed, if one considers that the bandwidth used was about 10 times larger than the optimum bandwidth.

For the critical ion number, below which thermal noise dominates the Poisson noise, Eq. (4.15)

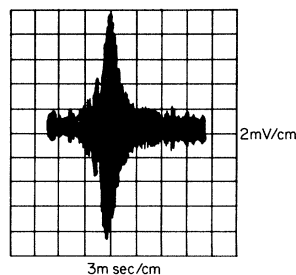


FIG. 15. Thermal ion-number signal. Without excitation of the ion motion, the induced voltage in a fixed tuned circuit is observed, when sweeping the macro-motion frequency through resonance. Experimental parameters: $V_0 = 137$ V_{peak}, $U_0 = 0$ V, $U_S = -2.5$ V, $i_e = 10$ mA, $T_e = 80$ msec, sensitivity 2 mV/cm, amplification 2000, total sweep period 32 msec.

gives $n_m = 10^4$. In the presence of the weak polarized Cs beam, the lifetime was reduced to 400 msec, mainly by rf heating collisions⁴ and by charge-exchange processes. After 800 msec of interaction time between the Cs beam atoms and the stored ions, the ion number had decreased to about 1/10 of the initial value, but additional fluctuations attributed to the Cs beam appeared. For this situation, the fluctuations of the ion-number signal, comparing consecutive signals, were 400:1.

C. Effect of the Ion Space Charge

The space charge of the ions slightly modifies the pseudopotential. However, an exact treatment of the problem is complex and would involve the knowledge of individual ion orbits.

In order to derive a value of the correct order of magnitude, we assume a spherical charge distribution and zero dc bias voltage. A more detailed analysis, using the actual ellipsoidal ion cloud and an additional dc voltage, is given elsewhere.⁵ If a uniform charge distribution of density \bar{n} in a trapping region of radius z_0 is assumed, the space-charge effect is equivalent to an additional dc bias voltage U_i . The space charge is defocusing in all directions, which means that the virtual bias voltage U_i has a different sign for the r and z directions. With this approximation, U_i follows from the Poisson equation to

$$U_i = \pm \bar{n} z_0^2 / 4\epsilon_0, \quad (4.17)$$

where ϵ_0 is the permittivity constant. Using the smallest characteristic dimension $z_0 = 25\text{mm}$ of the trap structure, we find

$$U_i = 2.8 \times 10^{-6} \bar{n}. \quad (4.18)$$

The influence of the ion space charge may be used to determine approximately the stored-ion charge. The procedure is outlined in the following.

The trap parameters were chosen to store both ${}^3\text{He}^+$ and a small number of H_2^+ test ions. Then the H_2^+ ion-number signal was detected in the conventional way by observing the damping of a tuned detection circuit at $\bar{\omega}_z(\text{H}_2^+)$, when the fundamental ion oscillation frequency was varied through resonance. In addition, all ${}^3\text{He}^+$ ions could be driven out of the trap by a strong rf pulse at $\Omega + \bar{\omega}_z({}^3\text{He}^+)$. The amplitude of this clearing pulse was adjusted before the actual measurement, by making the ${}^3\text{He}^+$ ion signal disappear. If now the ${}^3\text{He}^+$ ions were completely thrown out in every other detection cycle, the observed H_2^+ signal appeared space charge shifted during one cycle and unshifted in the following cycle. From the size of the shift, when interpreted as an additional dc bias voltage, the ${}^3\text{He}^+$ ion number is derived. With respect to the \bar{D}_z change, the measured shift was equivalent

to an applied dc voltage $U_i = 400$ mV, or, according to Eq. (4.18), was caused by a space charge of density $\bar{n} = 1.4 \times 10^5$ ions/cm³. The total number of stored ions follows to $n = 8 \times 10^6$, if the assumption of a uniform charge distribution over the trapping region of radius $z_0 = 25$ mm is taken into account. Care was taken to obtain a large amplitude of the H_2^+ oscillation for the purpose of averaging the space charge of the whole ${}^3\text{He}^+$ cloud.

It is interesting to compare this result with those derived from the ratio of the ion-number signals measured with and without coherent excitation. This ratio is

$$\left(\frac{S_c}{S_i}\right)^2 = n \bar{W}_c / \bar{W}_c \approx n(t_d/t_n)(ne\bar{D}/\bar{W}_1). \quad (4.19)$$

Assuming $\bar{W}_1 = ne\bar{D}$. Using the observed signal heights of Figs. 14(a) and 15, the measured values are

$$\frac{S_c}{S_i} \approx 1.4 \times 10^3, \quad t_d/t_n = \frac{1}{40}$$

from which the amount of the stored charge follows to $n \approx 8 \times 10^7$ ions, which seems to indicate that the actual values may be longer for t_d and shorter for t_n than those listed in Table III.

V. MEASUREMENTS

A. Detection Procedure

In most measurements, an ion-number signal was observed periodically at intervals of 1 sec. Figure 16 illustrates the typical sequence of manipulating pulses. A period of operation began by ensuring that the trap contained no charge. A short, intense, negative pulse throws out any ions, which might still be in the trap from the previous cycle. After this clearing pulse, an electronic delay from a master time base triggered the electron beam on for 80 msec. The master time base was synchronized to the mains. The electron beam ion-

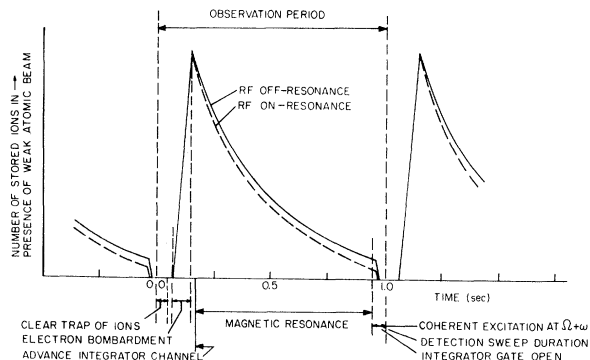


FIG. 16. Time evolution of stored ${}^3\text{He}^+$ charge in periodic sequence of manipulating pulses to observe induced magnetic dipole transitions.

ized the ${}^3\text{He}$ background gas so that ${}^3\text{He}^+$ ions were formed inside the trap. The ion-number signal could now be determined at variable times. Normally, the motional macromotion frequency $\bar{\omega}_z$ was set about 10 kHz below the detection frequency ω_0 . To sweep $\bar{\omega}_z$ through resonance, a linear negative-going dc sweep was applied to the ring electrode. Simultaneous with the detection sweep, another pulse at the sideband frequency $\Omega + \omega_0$ coherently excites the ion macromotion when $\bar{\omega}_z = \omega_0$, finally driving the ions against the electrodes. Hereby, an emission signal voltage is induced, which, after narrow banded amplification, is rectified and displayed on a scope.

To measure, for instance, the ion lifetime T_i , the period between ion formation and detection was varied in consecutive cycles. For ${}^3\text{He}^+$ ions, the decay of the motional ion resonance signal indicated a characteristic lifetime $T_i = 25$ sec. Even in a vacuum of roughly 1×10^{-10} Torr this lifetime was mainly determined by collisions with rest gas particles accompanied by rf heating. In the presence of the polarizing weak Cs beam, the lifetime is shortened to $T_0 = 0.4$ sec. For the purpose of comparing the two lifetimes, it was convenient to shut the Cs beam off by means of an electrostatically operated beam shutter.

The observation of induced magnetic dipole transition was made using data processing equipment in an integration scheme. Hereby, the lower part of the rectified ion-number signal, together with the noisy base line, was chopped off by suitably biasing the diode output (see Fig. 13). The resulting waveform was fed into a voltage to frequency converter, which produces a train of outgoing pulses. The number of pulses is proportional to the area of the ion-number signal. The pulses were counted and stored in one channel of a RIDL multi-channel memory system, type 24-2. The count gate was pulsed on only for the duration of the detection sweep, typically for a time of 32 msec. In such a measurement, the Cs beam passed through the trapping volume continuously. For the particular beam density chosen, detection was put into effect after a period of $2T_0 = 0.8$ sec, when, according to Eq. (2.8), an optimum signal-to-noise ratio is expected.

To avoid spurious resonances, it was advantageous to apply the hfs transition field pulsed, with transitions being induced only after the ions had been formed. In order to record a registration curve of induced magnetic dipole transitions, the frequency of the corresponding rf field was varied stepwise through resonance. In each step, the frequency was changed by a small amount and the corresponding ion-number signal was stored in a channel appointed before. In repeated sweeps through resonance, corresponding signals were fed into the same channels to achieve signal averaging.

B. Results

Magnetic dipole transitions were observed in two frequency regions. In order to induce the low-frequency Zeeman transition near 10 MHz, a rf field was generated in a single loop, rigidly mounted just outside the trap. The direction of the H_1 field was perpendicular to the static magnetic field. Figure 17 shows a display of the $\Delta F = 0$, $\Delta m_F = \pm 1$ hfs Zeeman transitions, which was obtained by varying the applied frequency step by step at a fixed static field of about 7.13 G. The display is the result of repeated measurements, when slowly sweeping 80 times through resonance, thereby integrating for a period of 2 h. The two outer signals correspond to d and f transitions. The signal in the center shows the double quantum e transition, which was used to implicitly determine the magnetic field in frequency units. The intensity of the d - and f -transition signals relative to the e -transition signal corresponds, ac-

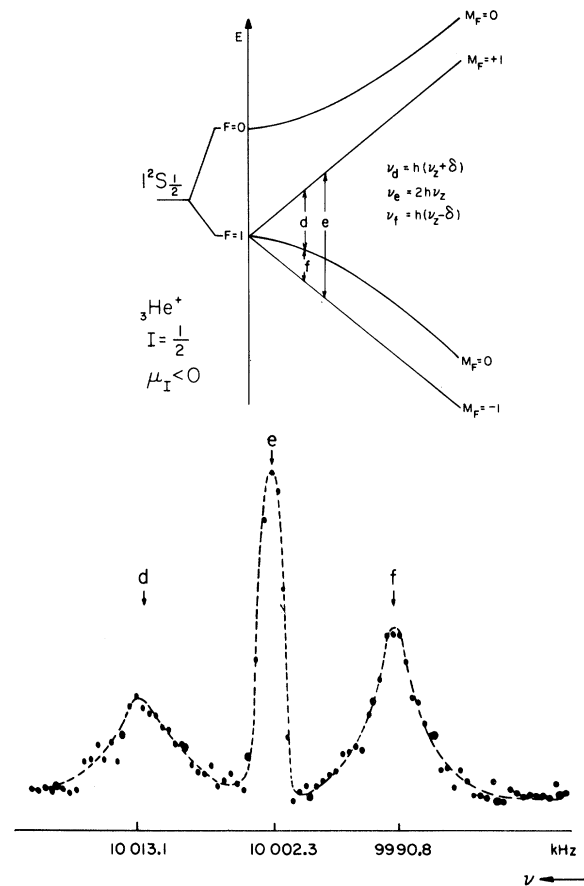


FIG. 17. Digital analyzer display of low-frequency ${}^3\text{He}^+$ resonances in a field of about 7.13 Oe, obtained in a 2-h run. For this recording the amplitude of the rf field was increased to such a value that no further changes in the heights of the d , e , and f peaks occurred.

ording to Table I, to an ion polarization $p \approx \frac{1}{2}$.

An analysis of the experimental signal intensity $S = 0.02$ on the basis of Eq. (2.8) and of the theoretical values of the cross sections for charge exchange shows that spin-independent processes are about 10 times more effective in reducing the ion number than charge exchange collisions with Cs alone.

The field-dependent a - and c -microwave transitions were observed with comparable intensities, as were the low-frequency transitions. Measurements have been made with the ion polarization being either positive or negative. A typical display of the c -transition signal is shown in Fig. 18. The structures in the resonance transition signal are Doppler sidebands caused, as mentioned above, by the Larmor precession of the ions. Additional sidebands being separated by the various harmonics of the ions macromotion from the central resonance signal have also been detected.

It should be noted that the occurrence of sidebands does not influence the accuracy of the measurements. This is clearly evident for the b transition, when comparing the linewidth of 10 Hz, with the separation of the closest sidebands being about 3.5 kHz for the Larmor sidebands, and a-

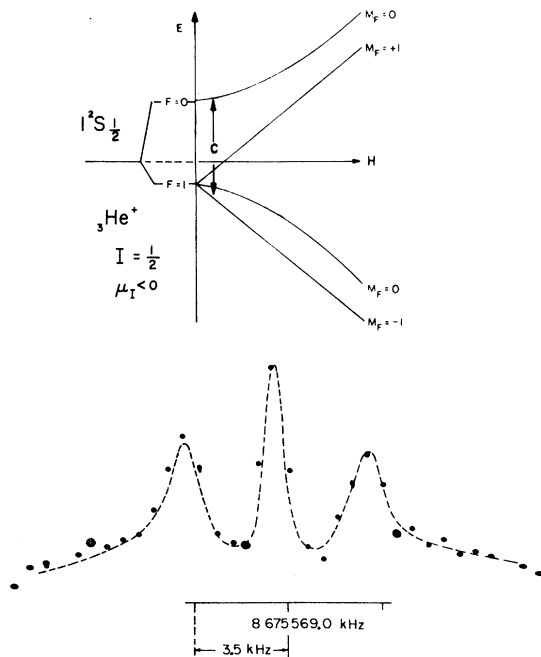


FIG. 18. Digital analyzer display of the microwave c transition near 8.6 GHz in a field of about 7.13 G. The symmetric sidebands are caused by mixing of the Larmor frequency. The static magnetic field is inclined by $\frac{1}{4}\pi$ with respect to the trap axis. The recording time was 2 h.

bout 60 kHz for the first motional sidebands distant from the central resonance peak.

The field insensitive b transition was of primary interest for the determination of the zero hfs splitting $\Delta\nu$. The consecutive-pulse multiple-resonance scheme, together with a very weak Cs beam, were used to observe this transition between practically pure states. The experimental procedure for setting up the consecutive-pulse multiple-resonance scheme was as follows. In previous experiments, the proper power levels for the 180° pulse at the d transition and the saturation pulse at the c transition frequency had already been determined. They were applied at the resonance frequency while the frequency of the b transition field was varied. The various resonance frequencies for the pulsed scheme were measured before and sometimes after each b -transition run. When alternately observing e -, c -, and b -transition resonance signals, it was possible to account for small daily drifts in the magnetic field.

A single determination of the b -transition frequency consisted of observing the signal intensity at typically 20 different frequencies spread at equal intervals over a region somewhat wider than the magnetic resonance curve. A display of the b transition, obtained over an integration period of 8 h is presented in Fig. 19. The frequencies have been chosen to observe signal amplitudes symmetric to the midpoint of the resonance. The center of the line was visually determined from the positions of two corresponding points, one on either side of the resonance, and of the point close to the signal center. The arithmetic mean value of such determinations for a single run was then corrected to account for a small frequency offset (in the order of several parts in 10^{-11}) between the local frequency standard and the 60 kHz WWVB signal received.

Table IV presents data collected in eight runs. The first column contains the arithmetic mean values for the position of the center of the b transition. The linewidths are given in the second column. The variation reflects measurements performed with different power settings and b -transition pulse lengths. For the three narrowest signals with a linewidth of about 10 Hz, minimum rf power and a pulse length of 76.6 msec were used. Column three indicates the position of the double quantum e transition, which may be considered as the calibration of the magnetic field. The Paschen-Back-Goudsmit shift δ needed to relate the b transition to $\Delta\nu$, the zero-field hfs splitting, amounted to about $\delta = 11.51$ kHz and could be determined in any particular measurement from the position of the double quantum e transition to within ± 1 Hz. Finally, the resulting zero-field hfs splitting $\Delta\nu$, derived by subtracting 2δ from the b -transition resonance frequency, is

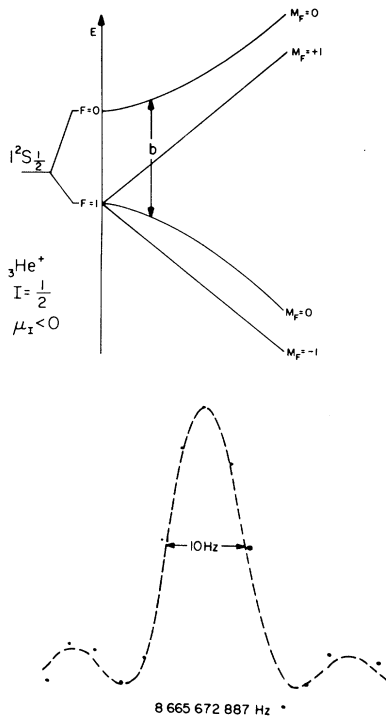


FIG. 19. Display of the b transition. The dashed curve is the theoretical line calculated for optimum perturbation $\gamma H_1 T_p = \pi$.

listed in the last column. The average mean value of the eight runs weighted according to the relative linewidth is also given. The limit of error reflecting the over-all accuracy has been taken as the maximum deviation of the individual measurements, to allow for possible systematic errors.

A systematic search for shifts in the order of a fraction of the linewidth has not yet been made.

However, so far no indication of a shift was found, when decreasing the b -transition power by an order of magnitude.

In principle, the b transition is expected to be broadened and shifted by the second-order Doppler effect, the spin exchange with Cs atoms, and by the Stark effect of the containing fields. From the discussion of the sizes of the various effects given in Secs. VI and VII, it follows that the present accuracy is mainly limited by the uncertainty in the energy distribution of the stored ions, reflecting itself in the second-order Doppler correction. Assuming that the ion orbits are large enough to sample the whole trapping volume, the relevant average ion energy is taken as roughly 0.4 times the depth of the smallest potential well, which is \bar{D}_p . According to Eq. (6.5), a second-order Doppler shift of +4 Hz was, therefore, applied to the weighted mean value, yielding the final result for the zero-field hfs splitting

$$\Delta\nu(1s^2S_{1/2}) = (8\,665\,649\,867 \pm 10) \text{ Hz.} \quad (5.1)$$

In this value, the error limit has been extended to include an estimated uncertainty of the second-order Doppler correction.

VI. DISCUSSION OF POSSIBLE FREQUENCY SHIFTS

In the ideal case, one would like to measure the transition frequency between the hyperfine sublevels of the ions at rest in free space. The goal of the present experimental effort with stored ions is to approach this ideal as closely as possible. In the actual case thus far, however, the ions are in motion and are not totally free from interaction with their environment. Hence, certain small frequency shifts are possible, which are analyzed in the following paragraphs. It will be seen that

TABLE IV. Summary of results (frequencies in Hz) of the ${}^3\text{He}^+$ ground-state hfs spectrum.

Field-independent transition ν_b : $(0, 0) \leftrightarrow (1, 0)$	Linewidth	Double quantum transition ν_e : $(1, 1) \leftrightarrow (1, -1)$	hfs splitting $\Delta\nu$
8 665 672 881.3	22	10 011 43	8 665 649 861
8 665 672 887.2	28	10 010 93	8 665 649 864
8 665 672 886.5	14	10 010 77	8 665 649 864
8 665 672 886.7	14	10 010 61	8 665 649 865
8 665 672 887.8	10	10 010 48	8 665 649 867
8 665 672 884.0	11	10 010 44	8 665 649 863
8 665 672 883.9	13	10 010 28	8 665 649 863
8 665 672 880.0	10	10 010 17	8 665 649 860
Weighted mean value = 8 665 649 863 (4)			
(A contribution of +4 Hz to account for the second-order doppler shift is included)			

$$\Delta\nu({}^3\text{He}^+, 1s^2S_{1/2}) = 8\,665\,649\,867(10) \text{ Hz}^a$$

^aSee Ref. 26.

those shifts which are not already of negligible size can be further reduced by orders of magnitude by contemplated improvements.

A. Stark Effect of the Containing Electric Fields

The hfs frequency of an atomic system placed in an external electric field E is Stark shifted to lowest order by a fractional amount kE^2 , where k may be evaluated exactly for a hydrogenlike system, in which case $k=16a^4/Z^6e^2$ where Ze is the nuclear charge and a is the Bohr radius.^{11, 12} For a typical trapping electric field of $V_{rms}=60$ V/cm (0.2 esu), the fractional shift in ${}^3\text{He}^+$ is thus 3×10^{-17} and is clearly negligible.

The near absence of shifts due to the containing fields is one of the major advantages of the ion-storage method. Buffer gases or inert walls¹³ used for containing neutral particles cause fractional shifts varying from 10^{-9} to 10^{-11} .

B. Dependence on External Magnetic Fields

By selecting $\Delta m_F = 0$ transitions one reduces the dependence on the magnetic field H to a relatively small calculable second-order contribution, which in the case of the ${}^3\text{He}^+$ ion produces a frequency shift $\delta\nu/H^2 = 452$ Hz/G² as shown in Sec. II A.

In the present experiment, a field of about 7 G was used leading to a $\delta\nu$ of about 23 kHz which could be determined to within about 1 Hz by measuring the Zeeman transitions as discussed in Sec. V D. By the use of magnetic shielding, however, the magnetic field in the vicinity of the trap may be reduced to less than 0.1 mG with enough homogeneity to keep the frequency of the Zeeman transitions well above their width. For such conditions $\delta\nu$ will be less than 10^{-5} Hz, corresponding to a fractional shift in the hfs of less than 10^{-15} .

C. Motional Magnetic Field

As an ion moves with velocity \vec{v} through the containing electric field $\vec{E} = \vec{E}_{rf} + \vec{E}_{dc}$, it experiences a motional magnetic field given by

$$\vec{H}_{mot} = \vec{v} \times \vec{E}/c, \quad (6.1)$$

where \vec{E} is in esu, \vec{H}_{mot} is in G. The presence of H_{mot} together with the applied external field H_0 leads to a change in the hfs frequency of an ion

$$\begin{aligned} \delta\nu &= a\langle H^2 \rangle = a\langle H_0^2 + 2\vec{H}_0 \cdot \vec{H}_{mot} + H_{mot}^2 \rangle \\ &= aH_0^2 + \delta\nu_{mot}, \end{aligned} \quad (6.2)$$

where, as in Sec. VI B, $a=452$ Hz/G² and the indicated averaging is taken with respect to time.

Terms linear in E_{rf} average to zero, with the result for the remaining terms

$$\delta\nu_{mot} = 2a\langle \vec{H}_0 \cdot \vec{v} \times \vec{E}_{dc}/c \rangle + a\langle (\vec{v} \times \vec{E}/c)^2 \rangle. \quad (6.3)$$

The first term on the right although linear in v does not necessarily average to zero for any given ion orbit. For example, referring to Fig. 6, consider an ion moving in a circular orbit of radius r in the xy plane at $z=0$. For such an orbit, the first term in Eq. (6.3) yields $\pm 2aH_{0z} vV_{dc} r/cr_0^2$ or, the sign determined by the sense of motion in the orbit. This term, however, does contribute a zero value when averaged over all of the different ions, which are just as likely to move in either sense of rotation. The term will therefore contribute a broadening of the resonance but not a shift, and is discussed in Sec. VII.

The last term in Eq. (6.3) does give a definite although small, resultant shift. Its magnitude may be estimated by using, as typical values for our trapped ${}^3\text{He}^+$ ions, $v=3 \times 10^6$ cm/sec, $r_0=3.6$ cm, $V_{rf}=137$ V=0.44 esu. Thus

$$\delta\nu_{mot} \simeq a(vV/cr_0)^2 \simeq 7 \times 10^{-8} \text{ Hz}$$

which is a totally negligible shift.

D. First-Order Doppler Shift

Suppose an ion with a hfs frequency ν_0 in its rest frame is oscillating with a definite frequency ν_i in a confined space of dimensions r_0 . As a result of the first-order Doppler effect,¹⁴ the ion will emit or absorb radiation at the frequency ν_0 , and at sideband frequencies $\nu_0 \pm n\nu_i$ differing from ν_0 by integral multiples of ν_i . The relative strength of the sidebands will be large when $r_0 \gg \lambda_0$ and will be small when $r_0 \ll \lambda_0$. We have already mentioned the observation of such sidebands (Sec. V B).

Of interest in this section is the possibility of a shift in the center frequency which is nominally at ν_0 . A small shift can occur if the ions have net translational velocity, as for instance, if they are created in one part of the trap and relax in another part. This shift can be analyzed in a manner similar to that employed for such an effect in the atomic hydrogen maser.¹³ If the ions are created at one end of the trap and relax at the other end (the worst possible case), the relative shift is

$$(\nu - \nu_0)/\nu_0 = 4\pi/3 \nu_i \tau^2 \nu_0, \quad (6.4)$$

where τ is the radiation lifetime of the ions. For $\tau = 30$ msec, corresponding to the 10-Hz line-widths observed, $\nu_i \simeq 60$ kHz = $\bar{\omega}_r/2\pi$, we have $(\nu - \nu_0)/\nu_0 \simeq 10^{-12}$. This shift will be much smaller

when longer lifetimes τ are used. Thus, $\tau = 1$ sec yields a relative effect of 10^{-15} . To the extent that the microwave field is in the form of standing waves in the trap rather than running waves, this shift is still further reduced.

E. Second-Order Doppler Shift

The second-order Doppler effect does not average in the same manner as the first-order effect because of its dependence on the square of the velocity. The fractional shift introduced by this effect is

$$(\nu - \nu_0)/\nu_0 = -\frac{1}{2} v^2/c^2 = \langle E_t \rangle / E_0, \quad (6.5)$$

where $\langle E_t \rangle$ is the average kinetic energy of each ion in the trap, and $E_0 = mc^2$ is their rest energy. Assuming $\langle E_t \rangle$ equal to $0.4\bar{D}_r = 1.2$ eV, where \bar{D}_r is the depth of the lowest trapping well, one obtains for ${}^3\text{He}^+$

$$(\nu - \nu_0)/\nu_0 = -4.4 \times 10^{-10}$$

This shift presents the most serious problem affecting the precision attainable with the ion-storage method. Work is underway to reduce this shift by cooling the ions to room temperature or lower.¹⁵ As a function of the absolute temperature T_i and atomic mass M of the ion, the shift is

$$(\nu - \nu_0)/\nu_0 = -1.4 \times 10^{-13} T/M. \quad (6.6)$$

At room temperature, the effect for ${}^3\text{He}^+$ is -10^{-11} , and for a heavier ion it can be much less, e.g., for Hg it is $\approx -10^{-13}$. By stabilizing the final ion temperature, one might be able to control this contribution. A small calculable correction applied to the measured frequency can then account for the second-order Doppler shift.

F. Spin Exchange Shifts

An order of magnitude estimate of spin-exchange shifts may be obtained as follows. Assuming unpolarized Cs atoms and ${}^3\text{He}^+$ ions, the collisions result in the formation of short-living complexes of which $\frac{3}{4}$ are in the triplet state and $\frac{1}{4}$ in the singlet state. The hfs associated with the ${}^3\text{He}$ nucleus in the triplet molecular complex is essentially the same as in the free ion, while this hfs vanishes for the singlet state. Consequently, the ${}^3\text{He}^+$ ions moving through a Cs beam of particle density N will have their hfs turned off for a small fraction of the time f . The observed average transition frequency is then shifted to lower values by a relative amount f . For f we take $\frac{1}{4}$ of $N \times \frac{4}{3} \times \pi r_{\text{SE}}^3$, the fractional spin-exchange volume, where r_{SE} is defined by $\pi r_{\text{SE}}^2 = 2Q_e$. As a numerical example, take $N = 10^8$ particles/cm³ and

$2Q_e = 1.4 \times 10^{-14}$ cm².¹⁶ Then $f \approx 10^{-13}$ is the fractional spin-exchange shift. As the beam intensity is reduced for longer ion lifetimes, this shift will be correspondingly smaller.

VII. CONTRIBUTION TO LINEWIDTH

In general, any process which limits the radiative lifetime of the stored ions will contribute to a broadening of the resonance line. Analyzed below are a number of such relaxation mechanisms. Their resultant contribution to the linewidth will be determined by the total relaxation rate which is the sum of the individual rates for each process. In addition, a spread in resonant frequencies among the ions, for example, due to magnetic field inhomogeneities, will broaden the resonance line. Such effects are also included in the discussion below.

A. Ion-Storage Time

At the operating background pressures of 10^{-9} Torr, normally encountered when the Cs beam was turned off, ${}^3\text{He}^+$ ions have been trapped for about 20 sec, which broadens the resonance line by a relative amount $1/\nu_0 \pi \tau = 2 \times 10^{-12}$. By cooling the ions and using lower pressures, ion storage times have been increased to greater than 10^4 sec, which makes this source of broadening totally negligible.

B. Magnetic Field Broadening

From Sec. VI B, a magnetic field inhomogeneity ΔH in a total field of H G causes a frequency width in Hz of $\Delta\nu_b = 904H\Delta H$, ignoring the effects of motional narrowing. In the present experiment, $\Delta H < 10^{-5} H$ over the ion trapping volume (see Sec. III D), and consequently in the 7.13 G field used, the linewidth contribution from field inhomogeneities should be less than 0.4 Hz. By the use of magnetic shielding as pointed out in Sec. VI B, H and ΔH may be reduced to below 0.1 mG, reducing the relative broadening to less than 10^{-15} .

Hum magnetic fields were also present, and broadened the field-dependent transitions by modulating the resonant frequency. In general, such broadening will occur¹⁴ if the depth of modulation $\Delta\nu_m$ is considerably greater than the hum frequency of 60 Hz (as is the case with the field-dependent transitions for which $\Delta\nu_m \approx 3$ kHz for the typical hum fields ΔH_m of 2 mG in the trap region). The hum fields have a considerably smaller effect on the b transition, for which $\Delta\nu_m = 904 H \Delta H_m \approx 6$ Hz which is $\ll 60$ Hz and thus will produce only a small amplitude in the 60-Hz sidebands. Further reduction can be achieved by magnetic shielding.

A similar shift results from any rf magnetic

fields that might be present, such as those (of order V_0/Z_0) associated with the trapping electric potential V_0 . For $V_0=150$ V and Ω equal to 1 MHz, the shift due to these rf fields is about 10^{-5} Hz which is negligible.

As indicated in connection with Eq.(6.3), there will be some broadening of the resonance due to the motional magnetic fields, of a maximum magnitude $2aH_0\nu V_{dc}/c\gamma_0 = 10^{-2}$ Hz for $H_0 = 10$ G and $V_{dc} = 10$ V = $1/30$ esu. By using small values of H_0 , this broadening may be reduced to an insignificant level.

C. Doppler Broadening

The first-order Doppler shift was shown to be negligible in Sec. VI C and thus the broadening is negligible also.

The second-order Doppler shift introduces a broadening to the extent that the ions have different average energies of motion. Thus, from Eq. (6.5), $\Delta\nu \approx \Delta E_t / E_0$, where ΔE_t is the spread in energies of the ensemble of ions. At worst, $\Delta E_t \approx \langle E_t \rangle$ in which case the Doppler width has the same magnitude as the second-order shift calculated in Sec. VI E. As indicated in that section, this effect can be significantly reduced by cooling the ions. In the present experiment, where the motional randomization time t_d is much shorter than T_b , the characteristic time for the b transition, considerable energy averaging may greatly reduce this type of broadening.

D. Interaction with Atomic Beam

The spin orientation of the ions is changed by spin exchange with the atomic beam. The spin-exchange relaxation time determines a further broadening of the resonance. In the present experiment the spin-exchange time was about 90 msec and thus contributed about 3 Hz to the total linewidth of 10 Hz. When the level of broadening due to other mechanisms, e.g., second-order Doppler effect, etc., is reduced, the spin-exchange time may be increased in the same proportion by reducing the Cs beam without reducing the size of the resonance signal. Hence, the spin exchange will not offer a serious limitation on the linewidth.

VIII. COMPARISON WITH THEORETICAL CALCULATIONS OF hfs SPLITTING

A. Ground-State Splitting Including Nuclear Structure

$^3\text{He}^+$ was selected as the first ion for precise study by the ISEC method because it is a simple one-electron system for which accurate calculations of the hfs may be carried out and compared with our experimental value. Considering the

electron and nucleus as point dipoles of magnetic moments μ_e and μ_n ; that is, ignoring the effects of nuclear structure, the following expression good to a few ppm has been derived¹⁷ for the hfs splitting in the ground state of a one-electron system of nuclear charge Z

$$\Delta\nu = \frac{16}{3} Z^3 \alpha^2 c R_\infty (\mu_n / \mu_e) [1 + m/M]^{-3} [1 + \alpha/2\pi + 0.328\alpha^2/\pi^2] [1 + \frac{1}{2} 3(Z\alpha)^2] [1 - \alpha^2 Z(\frac{5}{2} - \ln 2)], \quad (8.1)$$

where R_∞ is the Rydberg constant, the first bracket is the reduced mass correction, the second bracket is the anomalous electron magnetic moment contribution, the third bracket is the relativistic Breit correction, and the fourth bracket is the radiative correction of Kroll and Pollack. For accurate comparisons between the hfs values in the 1S and 2S states of $^3\text{He}^+$, further corrections to this expression are needed. These corrections are discussed in Sec. VIII B.

Substituting into the above expression for $\Delta\nu$ the values of the known fundamental constants [for which we take 137.0350 (4) for the value of α^{-1}],¹⁸ and evaluating $\mu_n/\mu_e = (\mu_n/\mu_e)(\mu_p/\mu_e)$ from the measured ratios¹⁹ μ_n/μ_p and μ_p/μ_e we obtain the numerical value for $^3\text{He}^+$

$$\Delta\nu = 8667.75 \pm 0.05 \text{ MHz},$$

where the greatest uncertainty comes from the values of α and μ_n/μ_p . Comparison of $\Delta\nu$ with the experimental value $\Delta\nu_{\text{expt}}$ leads to the concept of the hyperfine anomaly δ defined by

$$\Delta\nu_{\text{expt}}/\Delta\nu \equiv 1 + \delta,$$

which measures the contribution of nuclear structure effects to the hfs. Using our measured value for $\Delta\nu_{\text{expt}}$,

$$\delta = -2.09 \pm 6 \text{ ppm}.$$

The value of δ may be calculated on the basis of the theory of the structure of the ^3He nucleus. The results of these calculations are summarized by Novick and Commins¹ and Greenberg and Foley.¹⁷

B. Ratio of $^3\text{He}^+$ hfs Splittings in 1S and 2S States

In Sec. VIII A, we have discussed methods of studying nuclear structure by the effects of this structure on the hfs splitting. In this section, we discuss a method of utilizing hfs measurements in $^3\text{He}^+$ to make an accurate test of quantum electrodynamics. For this purpose, a useful quantity is the ratio $\Delta\nu(2S)/\Delta\nu(1S)$, where $\Delta\nu(2S)$ is the hfs splitting in the metastable 2S state of

${}^3\text{He}^+$, measured by Novick and Commins,¹ and $\Delta\nu(1S)$ is the ground-state splitting which we have measured. In this ratio the nuclear structure effects cancel up to order (atom radius/nuclear radius)² $\approx 10^{-8}$, and thus the radiative and other purely electrodynamic corrections to the hfs may be checked to this order of accuracy.

First, we give a simple nonrelativistic argument to make plausible the above-mentioned cancellation of the nuclear structure effects. The radial hydrogenic wave function $R_n(r)$ for S states of principal quantum number n satisfies the radial Schrödinger equation

$$\frac{d^2}{dr^2} (rR_n) + \frac{2m}{\hbar^2} [V(r) - E_n] rR_n = 0, \quad (8.2)$$

where $V(r) = -Ze^2/r$. As $r \rightarrow 0$, we have the limiting equation

$$\lim_{r \rightarrow 0} \frac{d}{dr} R_n = \frac{mZe^2}{\hbar^2} R_n = \frac{Z}{a_0} R_n, \quad (8.3)$$

where a_0 is the Bohr radius.

Now, part of the effect of the nuclear structure of the hfs comes from averaging the Fermi contact term over the nuclear coordinates. Thus, $\Delta\nu(nS)$ is proportional to $\langle R_n(r)^2 \rangle_N$. Expanding about $r=0$

$$\begin{aligned} |R_n(r)|^2 &= |R_n(0)|^2 + 2R_n(0) \left. \frac{dR_n(r)}{dr} \right|_{r=0} \Delta r + \dots \\ &= |R_n(0)|^2 (1 + 2Z(\Delta r/a_0) + \dots) \end{aligned} \quad (8.4)$$

and thus the correction factor due to the finite extent of the nucleus is independent of the state n up to second order in $\Delta r/a_0$.

This simple picture is by no means complete. However, detailed evaluation of the hfs by Iddings and Platzman²⁰ does indeed demonstrate explicitly the cancellation of first-order nuclear structure effects.

Detailed calculations of the hfs ratio for hydrogenic systems have been carried out by Zwanziger²¹ and Sternheim.²² The amount by which the ratio should differ from the factor of 8 given by the Fermi contact term may be expressed in the following form:

$$8\Delta\nu(2S)/\Delta\nu(1S) = 1 + \frac{5}{8} (Z\alpha)^2 + \Delta, \quad (8.5)$$

where the $(Z\alpha)^2$ term is the Breit relativistic shift and

$$\Delta = [A(Z) - 5/16\pi]\alpha(Z\alpha)^2 + R(\alpha^2 m/M; Z). \quad (8.6)$$

The first term in Δ is the radiative correction of order α^3 , with the coefficient $A(Z)$ representing the contribution of the Lamb shift to this

ratio. According to Zwanziger,

$$A(Z) = 3.40 - 1.0514 \ln Z \pm 0.02,$$

with the uncertainty due to computer evaluation of a definite integral. The second term in Δ is a sum of reduced mass contributions of order $\alpha^2 m/M$, including such effects as nuclear recoil and perturbations of the hydrogenic wave functions by the hfs interaction. Sternheim has obtained an expression for this term which yields the numerical value for ${}^3\text{He}^+$

$$R(\alpha^2 m/M; Z=2) = 9.20 \times 10^{-8}.$$

Combining all the terms, the theoretical value of Δ for ${}^3\text{He}^+$ is

$$\Delta_{\text{theoret}} = (4.09 \pm 0.02) \times 10^{-6}.$$

Combining our experimental value for $\Delta\nu(1S)$ with that of Novick and Commins for $\Delta\nu(2S)$, the experimental ratio yields

$$\Delta_{\text{expt}} = (4.21 \pm 0.19) \times 10^{-6}.$$

There is good agreement between the experimental and theoretical values of the ratio to within the quoted uncertainties.

IX. FUTURE DEVELOPMENTS

The ISEC technique may be used for accurate measurements of hfs splittings and electron g factors in atomic ions, for magnetic resonance studies of simple molecular ions, and for development of high-precision atomic clocks.

hfs and g factor measurements are of particular interest in ions such as He^+ and Li^{++} with known, hydrogenlike wave functions which permit accurate theoretical calculations for comparison with experimental measurements. The ISEC method as applied in the present experiment on He^+ may be similarly applied to measuring the hfs of Li^{++} by using a polarized beam of either cesium or hydrogen atoms, for which the charge-exchange cross section with Li^{++} should be large and spin-dependent.²³ A further intriguing possibility is a highly accurate comparison of the electron g factors for the free electron, for He^+ and Li^{++} . Recent calculations indicate additional radiative corrections to the moment of the electron when it is bound in the Coulomb field of an atom or ion.²⁴

With more complex ions, accurate calculations of the hfs are not possible. However, the ratio of hfs splittings in different isotopes of the same element, having the same electron wave functions, leads to a measurement of the hyperfine anomaly⁸ which is a helpful tool in evaluating nuclear struc-

ture theories.

Another class of experiments is concerned with magnetic resonance studies of simple molecules. We have already succeeded in observing induced magnetic dipole transitions in the rotational ground state of H_2^+ .²⁵ In this particular case polarization has been achieved by spin exchange with a polarized Cs atomic beam. It seems possible to study in an analogous way the isotopic molecules HD^+ , D_2^+ , HT^+ , T_2^+ , and DT^+ . Such experiments would make it possible to determine hfs splittings of ion molecules with a precision so far not obtained in molecular spectroscopy.

A somewhat different application of the ISEC technique is in the development of high-precision atomic clocks. From the discussions under Sec. VI and VII, the attainment of a relative precision of 10^{-15} seems possible. As shown in Sec. VI D, the most serious source of imprecision, the second-order doppler effect, can be minimized by using heavy cooled ions. Suitable heavy ions with

$^2S_{1/2}$ electron configurations are Cd^+ and Hg^+ for which, respectively, Na and Li are suitable collision partners. In fact, for almost all ions of interest, the energy imbalance criteria⁷ for collisions are fulfilled by one or more of those atoms which are conveniently employed in atomic beams machines, e. g., the alkalis and atomic hydrogen. The orienting collisions with the light alkali atom should cool the ions to the temperature of the atomic beam and thus minimize the second-order Doppler shift and broadening.

ACKNOWLEDGMENT

The authors gratefully acknowledge the many contributions of Stephen Menasian to the development of the technique. Thanks are due to Dr. David Church, Dr. Gene McCall, and Klaus Zieher for helpful discussions. Jake Jonson constructed the glassware.

X. EXPLANATION OF SYMBOLS

A. Latin Letters

A	magnetic hfs coupling constant
a	transition probability parameter
$2b$	time-independent part of transition probability
C	capacitance
\bar{D}_r, \bar{D}_z	radial and axial well depths of pseudopotential
\bar{D}	well depth of pseudopotential for $\bar{D}_r = \bar{D}_z$
E	kinetic energy
$E_0(\bar{r}, \bar{z})$	electric field at guiding center
$E_1(x, y, z)$	amplitude of ion excitation field
$\Delta E_1, \Delta E_3$	difference in ionization energy for asymptotic charge-exchange states
F, I, J, S	angular momenta
$\bar{F}(\bar{z})$	restoring force
g_F, g_J, g_I'	spectroscopic splitting factors
H_0	external magnetic field
H_1	transverse rf field
$H_{l, m, n}$	symbol for cavity mode
I	ionization potential

i_e	electron current
i_i	induced current
L	inductance
m	mass of ion
m_F, m_I, m_J, m_S	magnetic quantum numbers
N	number of atoms
\tilde{N}	density of atoms
\underline{N}	rms noise
\underline{N}_f	experimental value of rms noise
\underline{N}_f0	rms noise without Cs beam present
\underline{N}_i	statistical rms noise
\underline{N}_t	thermal rms noise
n	ion number
\tilde{n}	ion density
n_i	occupation number of state i
n_{i0}	initial occupation number of state i
$n_{\alpha d}, n_{\beta d}, n_{\gamma c}, n_{\delta c}$	transition modified occupation numbers
n_m	critical ion number
P	electron polarization of atoms
p	electron polarization of ions
p_i	transition reduced polarization due to transition i ($i = a, b, c, d, e, f$)
\bar{p}_i	average transition reduced polarization
$p_\alpha, p_\beta, p_\gamma, p_\delta$	electron-spin polarization numbers
\bar{Q}	average charge-exchange cross section
Q_e	spin-exchange cross section
Q_1, Q_3	singlet and triplet charge-exchange cross section
Q_i	quality factor of stored ions
Q_t	quality factor of detection circuit
q	total stored charge
R_s	impedance of detection circuit

r_0	radius of ring electrode
\bar{r}	radial coordinate of guiding center
$S(p, P)$	polarization signal
$S^*(p, P)$	optimum polarization signal
S'_i	relative signal strength in basic scheme
S^\dagger_i	relative signal strength in pulsed scheme
\underline{S}	ion-number signal
$\underline{S}_c, \underline{S}_i$	coherent and incoherent ion-number signal
\underline{T}	room temperature
T_i	storage time of ions without Cs beam
T_0	storage time of ions with Cs beam
T_1	spin precession time
T_d	duration of 180° pulse at d -transition frequency
T_e	spin-exchange time
T_p	repetition period of consecutive-pulse multiple-resonance scheme
t	time
t_d	phase memory time of coherently excited ions
t_e	duration of electron pulse
t_s	duration of effective detection and excitation sweep
t_n	neutralization time for rf driven ions
t_{t0}	damping time of detection circuit
t_{zt}	radiative damping time of a single ion
U	voltage
U_0	amplitude of dc voltage
U_i	equivalent bias voltage of space charge
U_e	electron acceleration voltage
U_s	detection sweep amplitude
u, v, z'	coordinates in rotating reference frame
u_0	signal voltage of ion motion
u_{0f}	peak value of signal voltage

V_0	peak amplitude of rf voltage
$W_{\beta\delta}$	transition probability for induced magnetic dipole transitions
\bar{W}	total energy of ion sample averaged over $2\pi/\Omega$
\bar{W}_c, \bar{W}_i	coherent and incoherent ion energy
W_{tc}, W_{ti}	coherent and incoherent energy of detection circuit
\bar{z}	axial coordinate of guiding center
\bar{z}_0	axial trap dimension

B. Greek Letters

α	fine-structure constant
$\alpha, \beta, \gamma, \delta$	hfs Zeeman levels
γ	gyromagnetic ratio
Δ	increment
δ	magnetic field contribution to weakly field-dependent b transition
ϵ	parameter describing effect of weak b transition in pulse scheme
ϵ_0	permittivity constant
ξ	amplitude of micromotion at Ω
ξ_0	peak amplitude of micromotion
κ	amplitude parameter of ion motion sidebands
μ_0	Bohr magneton
μ_n	nuclear magnetic moment
ν	frequency
ν_0	center of transition frequency
ν_i	resonance frequency of transition i ($i = a, b, c, d, e, f$)
$\Delta\nu$	zero-field hfs splitting
ξ	transformed time
$\phi(\gamma, z)$	electrical potential distribution in ion trap
$\phi'(\bar{r}, \bar{z})$	dc contribution to potential well
$\psi(\bar{r}, \bar{z})$	pseudopotential
$\psi'(\bar{r}, \bar{z})$	composite pseudopotential
Ω	angular micromotion frequency

$\bar{\omega}_z$	angular macromotion frequency in z direction
ω_0	angular detection frequency
ω_1	angular frequency of macroscopic magnetization
ω_L, ω_L'	angular frequency of Larmor precession

*Supported by grants and contracts from the U.S. Army Research Office (Durham), the National Science Foundation, and the U.S. Office of Naval Research.

[†]Present address: Department of Physics, Texas A&M University, College Station, Tex. 77843.

¹R. Novick and E. D. Commins, *Phys. Rev.* **111**, 822 (1958).

²H. G. Dehmelt, *Phys. Rev.* **109**, 381 (1959).

³H. G. Dehmelt and F. G. Major, *Phys. Rev. Letters* **8**, 213 (1962).

⁴F. G. Major and H. G. Dehmelt, *Phys. Rev.* **170**, 91 (1968).

⁵H. G. Dehmelt, *Advan. At. Mol. Phys.* **3**, 53 (1967); **5**, 109 (1969).

⁶E. N. Fortson, F. G. Major, and H. G. Dehmelt, *Phys. Rev. Letters* **16**, 221 (1966); H. G. Dehmelt, *Proceedings of the International Symposium of the Physics of One- and Two-Electron Atoms, Munich, 1968* (North-Holland Publishing Co. Inc., Amsterdam, 1969).

⁷D. Rapp and W. E. Francis, *J. Chem. Phys.* **37**, 2631 (1962); see also J. R. Peterson and D. C. Lorents, *Phys. Rev.* **182**, 152 (1969).

⁸R. P. Feynman, F. L. Vernon, and R. W. Hellwarth, *J. Appl. Phys.* **28**, 49 (1957); for an additional discussion and further references see, for example, N. F. Ramsey, *Molecular Beams* (Oxford at Clarendon Press, Oxford, England, 1956), p. 118.

⁹E. Fischer, *Z. Physik* **156**, 1 (1959); W. Paul, O. Osberghaus, and E. Fischer, *Forschungsber. Wirtsch. Verkehrsministeriums Nord-Rhein-Westfalen* No. 415, 1958 (unpublished).

¹⁰L. D. Landau and E. M. Lifschitz, *Mechanics* (Per-

gamon Press, Inc., Oxford, 1960).

¹¹C. Schwartz, *Ann. Phys. (N. Y.)* **2**, 156 (1959).

¹²E. N. Fortson, D. Kleppner, and N. F. Ramsey, *Phys. Rev. Letters* **13**, 23 (1964).

¹³D. Kleppner *et. al.*, *Phys. Rev.* **138**, A972 (1965).

¹⁴R. H. Dicke, *Phys. Rev.* **89**, 472 (1953).

¹⁵H. G. Dehmelt and F. L. Walls, *Phys. Rev. Letters* **21**, 127 (1968); D. A. Church and H. G. Dehmelt, *J. Appl. Phys.* **40**, 3421 (1969).

¹⁶H. A. Schuessler (unpublished).

¹⁷D. Greenberg and H. M. Foley, *Phys. Rev.* **120**, 1684 (1960).

¹⁸E. R. Cohen *et. al.*, *Rev. Mod. Phys.* **27**, 363 (1955); S. L. Kaufman *et. al.*, *Phys. Rev. Letters* **22**, 507 (1969).

¹⁹H. L. Anderson, *Phys. Rev.* **76**, 1460 (1949).

²⁰C. D. Iddings and P. M. Platzman, *Phys. Rev.* **113**, 192 (1959).

²¹D. E. Zwanziger, *Phys. Rev.* **121**, 1128 (1961).

²²M. M. Sternheim, *Phys. Rev.* **130**, 211 (1963); H. C. Goldwire, *Phys. Rev. Letters* **18**, 433 (1967).

²³*Atomic Energy Levels*, Natl. Bur. Std. (U.S.) Circ. No. 467 (Government Printing Office, Washington, D. C., 1962).

²⁴S. J. Brodsky and R. G. Parsons, *Phys. Rev.* **163**, 134 (1967).

²⁵H. A. Schuessler, *Bull. Am. Phys. Soc.* **13**, 1674 (1968); H. A. Schuessler and H. G. Dehmelt, *Report of the First International Conference on Atomic Physics, New York, 1968* (Plenum Press, Inc., New York, 1968).

²⁶Our earlier value of Ref. 6 is $\Delta\nu = 8\,665\,549\,905(50)$ Hz.